IEEE Access
practical innovations : open solutions

Received February 22, 2014, accepted March 16, 2014, date of publication April 2, 2014, date of current version April 29, 2014.

Digital Object Identifier 10.1109/ACCESS.2014.2315523

A Geometric Approach to Head/Eye Control

BIJOY K. GHOSH[1], INDIKA B. WIJAYASINGHE[2], AND SANATH D. KAHAGALAGE[1]
[1]Department of Mathematics and Statistics, Texas Tech University, Lubbock, TX 79409, USA
[2]Department of Mathematics and Statistics, Sam Houston State University, Huntsville, TX 79401, USA

Corresponding author: B. K. Ghosh (bijoy.ghosh@ttu.edu)

This work was supported by the National Science Foundation under Grant 1029178.

ABSTRACT In this paper, we study control problems that can be directly applied to controlling the rotational motion of eye and head. We model eye and head as a sphere, or ellipsoid, rotating about its center, or about its south pole, where the axes of rotation are physiologically constrained, as was proposed originally by Listing and Donders. The Donders' constraint is either derived from Fick gimbals or from observed rotation data of adult human head. The movement dynamics is derived on $SO(3)$ or on a suitable submanifold of $SO(3)$ after describing a Lagrangian. Using two forms of parametrization, the axis-angle and Tait–Bryan, the motion dynamics is described as an Euler–Lagrange's equation, which is written together with an externally applied control torque. Using the control system, so obtained, we propose a class of optimal control problem that minimizes the norm of the applied external torque vector. Our control objective is to point the eye or head, toward a stationary point target, also called the regulation problem. The optimal control problem has also been analyzed by writing the dynamical system as a Newton–Euler's equation using angular velocity as part of the state variables. In this approach, explicit parametrization of $SO(3)$ is not required. Finally, in the appendix, we describe a recently introduced potential control problem to address the regulation problem.

INDEX TERMS Orthogonal group, quaternions, Riemannian metric, Newton-Euler's equation, Euler-Lagrange's equation, Listing's law, Donders' law, optimal control, potential control, regulation problem.

I. INTRODUCTION

We analyze the problem of controlling the pointing direction of a rigid body, actuated by controllers that rotate the body. Our motivation stems primarily from the problem of controlling the orientation of human head/eye complex (see [1] and [2] for an early reference to the eye and head movement problem, respectively), where the goal is to eventually point the head or the eye towards a point target. The target could be stationary or moving giving rise to, respectively, a *regulation* [3] or a *tracking* problem [4]. In this paper, we restrict ourselves to regulation problem only. In 3D, even after pointing towards a target, the orientation of a rigid body, being controlled, remains ambiguous. For the eye control problem, this is undesirable, particularly because while viewing an object, orientation ambiguity would imply that the image of a target would have rotational ambiguity on the retina. In order to handle the rotation ambiguity during the process of turning the head and the eye, the orientation space is often restricted in ways that will be discussed later in this paper. This fact was observed since 1845 by physiologists such as Listing [5], Donders [6] and Helmholtz [7], to name a few.

Simply speaking, Listing had observed that eye rotations are constrained to have only two degrees of freedom and their orientations are completely prescribed by their gaze directions. There is an alternative, but equivalent language to describe the Listing's constraint. It states that all possible orientations of the eye, away from the *primary position* (typically looking straight ahead), are obtained by rotating the eye about an axis of rotation restricted to a fixed plane that goes by the name **Listing's Plane** (see Fig. 1).

Complementary to the eye movement problem, Donders studied the possible orientations human head can attain, under

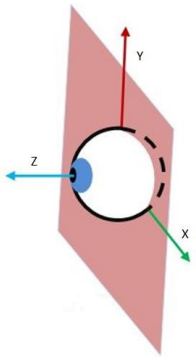

FIGURE 1. Listing's plane, fixed to the head, is shown along with eye in the primary gaze direction.

spontaneous head movement, and proposed that the 'axes of head rotations' (suitably scaled) away from a primary head position, is restricted to a fixed surface that goes by the name **Donders' Surface** [8]– [10] (see Fig. 2). In essence, Donders' law of head movement generalizes the Listing's Law of eye movement. Whereas the Listing's plane is fixed and is typically held constant,[1] Donders' surface is also assumed fixed but changes from one human subject to another [12], [13]. For the same physical task of 'head pointing', it follows naturally that two human subjects would orient their heads differently guided by their respective Donders' surfaces.

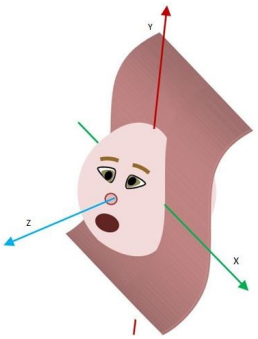

FIGURE 2. Donders' surface, fixed to the torso, is shown along with head in the primary pointing direction.

The control objective considered in this paper is to regulate the rotation of eye or head, i.e. to change the orientation from a given initial to a desired final gaze/pointing direction. The control problem is described under the assumption that the state space is the unconstrained $SO(3)$, or it is constrained to be a sub manifold *LIST* for the eye movement or *DOND* for the head movement. Although, typically we assume that the eye and head are spheres rotating about its center, we have also considered the case when they can be ellipsoidal and in the case of head, rotating about the south pole. Thus we simulate the problem when the head is rotating about the neck. The parameters of the ellipsoid is chosen to match roughly the size of an adult human eye and human head. Finally, two different Donders' constraints have been considered in this paper. The first one is the constraint arising from Fick gimbals and the second one has been borrowed from [13], where the parameters had been obtained from recorded human head movement data.[2]

In order to execute the task of rotation, suitably attached muscles produce torques. In the case of eye movement, three pairs of torque producing extra-ocular muscles, are recruited roughly along the three independent axes. Many previous, eye movement control studies have looked at detailed muscle models, as in [14]– [18]. A recent survey on the head movement control has been described in [19]. To simplify our presentation of the control problem in this paper, neuromuscular systems have not been looked at. We consider externally applied torques that are either in the form of **generalized torques**, tied to the parameters of the space of allowed orientations or in the form of **external torques** described with respect to the inertial frame. The torques are assumed unconstrained by the dynamics of muscles and neurons.

In sections II - V, this paper presents an overview from [4], [12], [13], and [20] in a tutorial style. We have introduced two parameterizations of S^3 and introduced the spaces LIST and DOND. Listing's and two versions of Donders' theorem are described in section IV.[3] These theorems characterize orientation ambiguity for a specified gaze/pointing direction. Riemannian metric and the corresponding geodesic equations are introduced in section V, for eye/head shaped like a perfect sphere. This assumption was relaxed in section VI, where a procedurally new approach to writing the Riemannian metric was introduced. Using the axis-angle and the Tait-Bryan parameters, we also compute the angular velocity vector and define kinetic energy using the angular velocity and the moment of inertia. In sections VII and VIII, eye and head movements are introduced as a dynamical system using respectively the Euler-Lagrange's equation and Newton-Euler's equation. Finally, section IX ends the paper by considering examples from optimal control. We add an appendix to talk about the potential control approach, which is particularly relevant for Lagrangian systems.

II. BACKGROUND GEOMETRY OF S^3 AND $SO(3)$

Since every orientation can be viewed as a point in $SO(3)$, eye and head movements can be described as trajectories in $SO(3)$, the space of rotations. Parametrization of points in $SO(3)$ can be easily obtained from a parametrization of S^3, the unit sphere in $\mathbb{R}^4$. We consider a map between S^3 and $SO(3)$ given by

$$rot : S^3 \to SO(3), \tag{1}$$

described as

$$\begin{bmatrix} q_0 & q_1 & q_2 & q_3 \end{bmatrix}^T \longmapsto Q, \tag{2}$$

where

$$Q = \begin{bmatrix} q_0^2+q_1^2-q_2^2-q_3^2 & 2(q_1q_2-q_0q_3) & 2(q_1q_3+q_0q_2) \\ 2(q_1q_2+q_0q_3) & q_0^2+q_2^2-q_1^2-q_3^2 & 2(q_2q_3-q_0q_1) \\ 2(q_1q_3-q_0q_2) & 2(q_2q_3+q_0q_1) & q_0^2+q_3^2-q_1^2-q_2^2 \end{bmatrix}. \tag{3}$$

The map '*rot*' in (1) is surjective but not $1-1$. This is because both $q = [q_0, q_1, q_2, q_3]^T$ and $-q$ in S^3 has the same image. The columns of the 3×3 matrix (3) are orthonormal and we shall interpret them as coordinates attached to the rotating body.[4] Additionally, we use the convention that the third

[1] Studies have indicated (see for example [11]), that Listing's plane tilts slightly with the changing orientation of the head. In this paper, we will not concern ourselves with this tilt.

[2] In [13], six Donders' surfaces were reported.

[3] It is unclear if Listing and Donders actually wrote these as theorems. What is clear, is that their intention was to restrict the orientation space is such a way that *gaze/pointing vector would uniquely specify the complete orientation.*

[4] The matrix Q describes the instantaneous orientation of the rigid body.

column is the 'gaze direction', when the rotating body is the eye. Likewise it is the 'pointing direction' for the head. We define the following projection map

$$proj : SO(3) \to S^2, \tag{4}$$

described as

$$Q \longmapsto \begin{bmatrix} 2(q_1q_3 + q_0q_2) \\ 2(q_2q_3 - q_0q_1) \\ q_0^2 + q_3^2 - q_1^2 - q_2^2 \end{bmatrix}.$$

The mapping 'proj' cannot be $1-1$ because the dimension of the domain is greater than the range. The following proposition due to Helmke [21] describes the pre-image of 'proj' as follows.

Proposition I (Helmke): Let us denote the composite map $proj \circ rot$ by L. If q and $\bar{q}$ are two unit quaternions, to be viewed as points in S^3, such that $L(q) = L(\bar{q})$, then there exists a unit quaternion of the form $u = (a, 0, 0, b)$ where $a^2 + b^2 = 1$ such that $\bar{q} = q \bullet u$. □

Remark I: Points in S^3 can be viewed as unit quaternions [22], [23], and we denote quaternion multiplication by the symbol $\bullet$. □

It follows that, Proposition I characterizes the orientation ambiguity for a specific heading (gaze) direction. Pre image of L is a circle in the space of all orientations. It was remarked in the introduction (section I), that an important problem in the physiology of human eye and head rotation is to be able to *disambiguate* the orientation ambiguity, during regulation. The eye (when head is fixed) and head (when torso is fixed) handle this problem by imposing Listing's and Donders' constraints, respectively.[5]

III. TWO PARAMETERIZATIONS OF S^3

The space $SO(3)$ of rotations can be parameterized in several ways. The possible candidates include Euler angles [24], Tait-Bryan angles [25], [26], axis-angle pairs [27], Euler-Rodrigues parameters [28], [29], an older name for the unit quaternion parameters [30] etc. The Euler angles and the Tait-Bryan angles are similar in the sense that they decompose a specific rotation as a cascade of three simple rotations. In these two parameterizations, the angles describe the amount of each simple rotations along a specific coordinate axis. Axis-angle representation, utilizes the fact that every rotation can be represented with respect to a unit axis vector by a specific angle in the anticlockwise direction. This idea is also utilized in Euler-Rodrigues parametrization (equivalently the quaternion parameters) where the unit axis vector is scaled by a trigonometric function of the rotation angle. The resulting 'rotation vector' can be identified as the homogeneous coordinates of a unit vector in $\mathbb{R}^4$, equivalently a point in S^3.

Remark II: In this paper, we do not use Euler angles to describe a point on $SO(3)$, because historically this has not been used in the literature on 'eye' and 'head' movements. Note that head movements are typically described using Euler-Rodrigues parameters [31], [32], whereas eye movements have been described in [12] and [20], using axis-angle pairs. □

As described in section II, our main interest is in parameterizing the space of orientations $SO(3)$. It turns out that it is much cleaner to parameterize S^3 instead, because of the map 'rot' (1). In this section we describe two alternative parameterizations of S^3, that have been used by the authors to study eye and head movement problems.

A. AXIS-ANGLE PARAMETRIZATION

We consider a parametrization of a point in S^3 using three angle variables θ, ϕ and α as follows[6]

$$q(\theta, \phi, \alpha) = \begin{bmatrix} \cos\frac{\phi}{2} \\ \sin\frac{\phi}{2} \begin{pmatrix} \cos\theta\cos\alpha \\ \sin\theta\cos\alpha \\ \sin\alpha \end{pmatrix} \end{bmatrix}, \tag{5}$$

where we assume $\theta \in [0, \pi]$, $\phi \in [0, 2\pi]$ and $\alpha \in [-\frac{\pi}{2}, \frac{\pi}{2}]$. Let us define

$$Q(\theta, \phi, \alpha) \;=\; rot(q(\theta, \phi, \alpha)). \tag{6}$$

By computing $w = Q(\theta, \phi, \alpha)v$, where v, w are vectors in $\mathbb{R}^3$, one can show that w is obtained by rotating v by an angle ϕ about the axis

$$\begin{pmatrix} \cos\theta\cos\alpha \\ \sin\theta\cos\alpha \\ \sin\alpha \end{pmatrix},$$

rotated in an anticlockwise direction. If we assume that $\cos\frac{\phi}{2} \neq 0$, one can normalize the homogeneous coordinates in (5) and obtain the vector

$$\zeta \;=\; \begin{bmatrix} \tan\frac{\phi}{2} \begin{pmatrix} \cos\theta\cos\alpha \\ \sin\theta\cos\alpha \\ \sin\alpha \end{pmatrix} \end{bmatrix}, \tag{7}$$

as coordinates of S^3 for this chart. The vector ζ in (7) will be called the *rotational vector*.[7]

B. TAIT BRYAN PARAMETRIZATION

In this subsection, we introduce the Tait-Bryan angles [25], [26], given by ϕ_1, ϕ_2 and ϕ_3, as follows

$$q(\phi_1, \phi_2, \phi_3) = \begin{pmatrix} \sin\frac{\phi_1}{2}\sin\frac{\phi_2}{2}\sin\frac{\phi_3}{2} + \cos\frac{\phi_1}{2}\cos\frac{\phi_2}{2}\cos\frac{\phi_3}{2} \\ \cos\frac{\phi_1}{2}\sin\frac{\phi_2}{2}\cos\frac{\phi_3}{2} + \sin\frac{\phi_1}{2}\cos\frac{\phi_2}{2}\sin\frac{\phi_3}{2} \\ \sin\frac{\phi_1}{2}\cos\frac{\phi_2}{2}\cos\frac{\phi_3}{2} - \cos\frac{\phi_1}{2}\sin\frac{\phi_2}{2}\sin\frac{\phi_3}{2} \\ \cos\frac{\phi_1}{2}\cos\frac{\phi_2}{2}\sin\frac{\phi_3}{2} - \sin\frac{\phi_1}{2}\sin\frac{\phi_2}{2}\cos\frac{\phi_3}{2} \end{pmatrix}, \tag{8}$$

where we assume that $\phi_1 \in [-\pi, \pi]$, $\phi_2 \in [-\frac{\pi}{2}, \frac{\pi}{2}]$, $\phi_3 \in$

[5]The scenario when eye and head are both moving has not been discussed in this paper, see [4].

[6]This parametrization has been introduced in [12].

[7]Rotational vectors will be used in defining Listing's plane and Donders' surfaces later in section IV

$[-\pi, \pi]$. These parameters were introduced in the context of head movement in [13]. Tait-Bryan parameters generalize a typical Fick gimbal system, [33], [34], which we now describe (see [35] for an earlier reference on Euler Angles).

A 2-gimbal system has two axes of rotations, where the assumption is that the first axis is fixed and the second axis rotates with the head, when the head rotates about the first axis. Subsequently, the head also rotates about the second axis. Following Fick gimbals, we assume that the fixed axis is the vertical axis, which is perpendicular to the ground and passes through the center of the head. The initial orientation of the second axis is horizontal and is perpendicular to the primary heading direction, also passing through the center of the head. We denote the anticlockwise rotation angle about the fixed (yaw) axis by ϕ_1, and the anticlockwise rotation angle about the nested horizontal (pitch) axis by ϕ_2. The roll is assumed to be zero and the final orientation of the head is a combination of the two rotations, yaw and pitch. If we define ϕ_i to be the angle of rotation with respect to the axis i, for $i = 1, 2, 3$, the nesting of the three axes is shown in Fig. 3a.

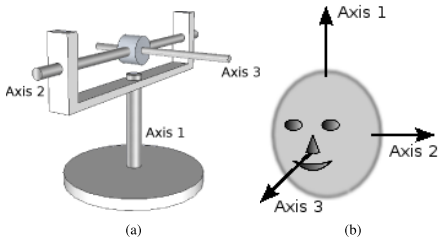

FIGURE 3. Tait-Bryan angles are ϕ_1, ϕ_2, ϕ_3, where ϕ_i is counterclockwise head rotation, with respect to axis i. (a) Generalized gimbal frame. (b) Head showing gimbal axes.

Tait-Bryan parametrization generalizes the gimbal system by introducing a third axis, initially along the line of gaze perpendicular to the vertical and horizontal axes of the gimbal system. We assume that the third axis rotates with respect to the first two axes of the gimbal system by angles ϕ_1 and ϕ_2 respectively. Finally we assume that the head rotates anticlockwise by an angle ϕ_3 with respect to the nested third (roll) axis. Quaternion representation of the Fick gimbals is given by

$$q(\phi_1, \phi_2) = \begin{pmatrix} \cos\frac{\phi_1}{2}\cos\frac{\phi_2}{2} \\ \cos\frac{\phi_1}{2}\sin\frac{\phi_2}{2} \\ \sin\frac{\phi_1}{2}\cos\frac{\phi_2}{2} \\ -\sin\frac{\phi_1}{2}\sin\frac{\phi_2}{2} \end{pmatrix}, \tag{9}$$

obtained by imposing $\phi_3 = 0$ in (8). Writing $q = [q_0, q_1, q_2, q_3]^T$ as in section II, it follows from (9) that for the Fick gimbals, we obtain[8]

$$q_0 q_3 = -q_1 q_2. \tag{10}$$

Remark III: If L is the composite map described in Proposition I, one can parameterize the gaze/pointing directions as

$$L(q(\theta, \phi, \alpha)) = \begin{pmatrix} \sin^2\frac{\phi}{2}\sin(2\alpha)\cos\theta + \sin\phi\cos\alpha\sin\theta \\ \sin^2\frac{\phi}{2}\sin(2\alpha)\sin\theta - \sin\phi\cos\alpha\cos\theta \\ \cos^2\frac{\phi}{2} - \sin^2\frac{\phi}{2}\cos(2\alpha) \end{pmatrix} \tag{11}$$

and

$$L(q(\phi_1, \phi_2, \phi_3)) = (\sin\phi_1\cos\phi_2, -\sin\phi_2, \cos\phi_1\cos\phi_2)^T. \tag{12}$$

Note that for the Tait-Bryan parametrization, the gaze vector is independent of the roll angle ϕ_3. This is intuitive because the roll, by definition, is rotation about the gaze directional axis. □

IV. THE SPACES LIST AND DOND

Listing's law asserts that, for eye movement, the rotational vector ζ in (7), is restricted to the plane, $\alpha = 0$, called Listing's plane. Equivalently, the axis of rotation is restricted to a fixed plane given by $q_3 = 0$. We define *LIST* to be the submanifold of S^3 and $SO_L(3)$ to be the submanifold $SO(3)$ satisfying the Listing's constraint. Using the axis-angle parametrization, we have the following sequence of maps

$$[0, \pi] \times [0, 2\pi] \times \left[-\frac{\pi}{2}, \frac{\pi}{2}\right] \xrightarrow{q} LIST \xrightarrow{rot} SO_L(3) \xrightarrow{proj} S^2 \tag{13}$$

defined by

$$(\theta, \phi, 0) \longmapsto \begin{pmatrix} \cos\frac{\phi}{2} \\ \sin\frac{\phi}{2}\cos\theta \\ \sin\frac{\phi}{2}\sin\theta \\ 0 \end{pmatrix} \longmapsto Q(\theta, \phi, 0) \longmapsto \begin{pmatrix} \sin\theta\sin\phi \\ -\cos\theta\sin\phi \\ \cos\phi \end{pmatrix},$$

and the following theorem due to Listing.

Theorem I (Listing): Under the Listing's constraint, the map

$$SO_L(3) - \left\{ \begin{pmatrix} \cos 2\theta & \sin 2\theta & 0 \\ \sin 2\theta & -\cos 2\theta & 0 \\ 0 & 0 & -1 \end{pmatrix} \right\} \xrightarrow{proj} S^2 - \left\{ \begin{pmatrix} 0 \\ 0 \\ -1 \end{pmatrix} \right\} \tag{14}$$

described by (13) is one to one and onto. □

Proof of the Listing's theorem has been sketched in [12]. If we choose the convention that $(0, 0, 1)^T$ is the frontal gaze direction, it would follow that $(0, 0, -1)^T$ is the backward gaze direction. Listing's theorem claims that for all but the backward gaze direction, every other gaze direction completely specifies the rotation matrix in $SO_L(3)$, hence the orientation of the eye.

Donders' law generalizes Listing's law by asserting that, for the head movement, the rotation vectors ζ in (7) are not spread out in a 3-D volume but instead fall in a single two-dimensional surface, known as the Donders' surface (see Fig. 2). Existence of a Donders' surface has been established in sufficient details in [9], [36], and [38]– [41]. It is observed

[8]This relation (10) has already been introduced in [36] and [37].

that the Donders' surface is a saddle shaped surface, with non-zero torsional component at oblique facing directions, obtained by mildly twisting a plane (see Fig. 4 for the Donders' surface (10) originating from Fick gimbals). Two Donders' surfaces reported in [13] have also been sketched in Fig. 5.

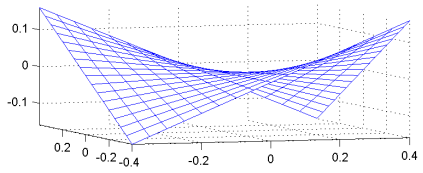

FIGURE 4. Donders' surface (10) corresponding to the Fick gimbal scaling q_0 in (2) to 1. The scaled coordinates are $\bar{q}_i = \frac{q_i}{q_0}$ for $i = 1, 2, 3$. The coordinate $\bar{q}_3$ along the vertical line shows the nonzero torsion. The horizontal plane is coordinatized by $\bar{q}_1$ and $\bar{q}_2$.

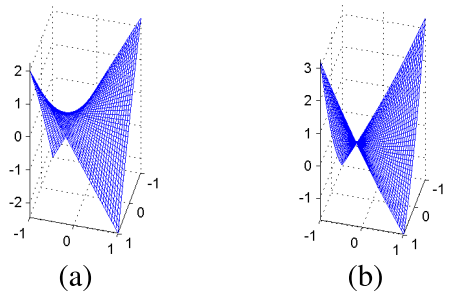

FIGURE 5. Using measured data on human head orientations, six Donders' surfaces have been displayed in [13]. In this figure, we display surfaces 2 and 13 and call them S2 and S13. The coordinate axes match Fig. 4 but are scaled differently. (a) Donders' surface S2. (b)Donders' surface S13.

At this point, it would be natural to ask what would be the appropriate generalization of the Listing's theorem in the case of *DOND*. As in *LIST*, we define *DOND* to be the submanifold of S^3 and $SO_D(3)$ to be the submanifold of $SO(3)$ satisfying the Donders' constraint. Using the axis angle parametrization, let us describe the Donders' surface (see [12]) by constraining α as

$$\alpha \ = \ \varepsilon \ \sin(2\theta), \tag{15}$$

and write down the *rotational vector* as

$$\zeta_{dond} \ = \ \left[\tan\frac{\phi}{2} \begin{pmatrix} \cos\theta\cos(\varepsilon\ \sin(2\theta)) \\ \sin\theta\cos(\varepsilon\ \sin(2\theta)) \\ \sin(\varepsilon\ \sin(2\theta)) \end{pmatrix} \right], \tag{16}$$

where the parameter ε is assumed to be a small positive or negative constant. The motivation to consider Donders' surface in the form (15) follows from [42], wherein the following was observed about a typical head movement

When the axis of rotation is horizontal or vertical (i.e. when θ is a multiple of $\frac{\pi}{2}$), head moves without any torsion. At other angles of rotation, there is a gradual increase in torsion.

As in (13), we have the following sequence of map

$$[0, 2\pi] \times [0, 2\pi] \ \stackrel{q}{\rightarrow} \ DOND \ \stackrel{rot}{\longrightarrow} \ SO_D(3) \ \stackrel{proj}{\longrightarrow} \ S^2 \tag{17}$$

defined by

$$(\theta, \phi) \longmapsto \begin{pmatrix} \cos\frac{\phi}{2} \\ \sin\frac{\phi}{2}\cos\theta\cos(\varepsilon\ \sin(2\theta)) \\ \sin\frac{\phi}{2}\sin\theta\cos(\varepsilon\ \sin(2\theta)) \\ \sin\frac{\phi}{2}\sin(\varepsilon\ \sin(2\theta)) \end{pmatrix}$$

$$\longmapsto Q(\theta, \phi, \varepsilon\ \sin(2\theta)) \longmapsto \begin{pmatrix} \Delta_1 \\ \Delta_2 \\ \Delta_3 \end{pmatrix},$$

where

$$\begin{aligned} \Delta_1 \ &= \ \sin\theta\sin\phi\cos(\varepsilon\sin(2\theta)) + \cos\theta\sin^2\frac{\phi}{2}\sin(2\varepsilon\sin(2\theta)) \\ \Delta_2 \ &= \ -\cos\theta\sin\phi\cos(\varepsilon\sin(2\theta)) + \sin\theta\sin^2\frac{\phi}{2}\sin(2\varepsilon\sin(2\theta)) \\ \Delta_3 \ &= \ \cos^2\frac{\phi}{2} - \sin^2\frac{\phi}{2}\cos(2\varepsilon\sin(2\theta)). \end{aligned} \tag{18}$$

The following theorem for the Donders' surface has been described in [12].

Donders' Theorem II: Under the Donders' constraint (15), the map *proj* in (17) is $2-1$, for all points in the range S^2 outside a closed and bounded set Ξ that contains the backward pointing direction. Furthermore, almost everywhere in Ξ the map *proj* is $4-1$. □

Sketch of the set Ξ from [12] is shown in Fig. 6. The size of the set Ξ is small, for small values of ε and when ε approaches 0 the set Ξ approaches the backward pointing direction. Moreover the map *proj* in (17), degenerates to a $1-1$ map. It would follow that Listing's theorem (Theorem I) is recovered in the limit when ε approaches 0.

Remark IV: Donders' surfaces described as in (15) were introduced in [12] for the first time. However, we would like to note that *under small angle hypothesis*, i.e. if the angles ϕ and α are sufficiently small, the Donders' constraint (10), arising from Fick gimbals, can be approximated as

$$\alpha \ = \ -\frac{1}{4}\phi\ \sin(2\theta),$$

which would be in the form (15), where $\varepsilon \ = \ -\frac{\phi}{4}$. □

In [31] and [32], Donders' surfaces are described as a quadratic surface using quaternion parameters q_0, q_1, q_2, q_3 from (2) as follows

$$\bar{q}_3 = h_0 + 2h_1\bar{q}_1 + 2h_2\bar{q}_2 + h_{11}\bar{q}_1^2 + h_{22}\bar{q}_2^2 + 2h_{12}\bar{q}_1\bar{q}_2, \tag{19}$$

where $\bar{q}_i = \frac{q_i}{q_0}$, $i = 1, 2, 3$. The quadratic surface representation of the Donders' surface has been subsequently used by the authors in [13]. Two of the surfaces are shown in Fig. 5. Using the Tait-Bryan parametrization (8), the Donders' surface equation (19) can be written as a quadratic equation in $\tan\frac{\phi_3}{2}$ given by

$$t\ \tan^2\frac{\phi_3}{2} \ + \ s\ \tan\frac{\phi_3}{2} \ + \ r \ = 0, \tag{20}$$

where t, s and r are functions of ϕ_1 and ϕ_2, detail derivation of which are omitted. For those angle variables ϕ_1, ϕ_2 for which $s^2 \ - \ 4\,t\,r \ \geq \ 0$, we solve ϕ_3 as a function of ϕ_1 and ϕ_2.

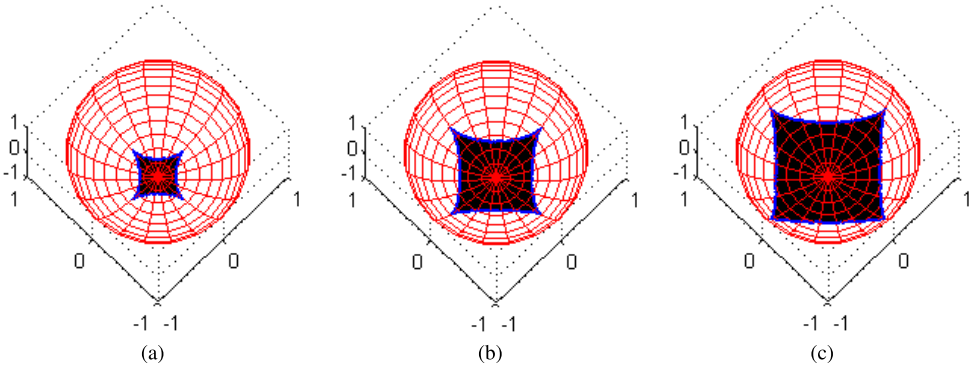

FIGURE 6. Backward pointing direction of the head is shown in the figure as the south pole. The shaded region Ξ around the south pole is the set of pointing directions where the number of possible orientations satisfying Donders' constraint is generically 4. Outside the shaded region Ξ, the number of possible orientations of the head for a specific pointing direction is two (counting multiplicities). The value of ε for the Donders' constraint (15) are shown in the captions above. (a) $\varepsilon = 0.1$. (b) $\varepsilon = 0.2$. (c) $\varepsilon = 0.3$.

When the discriminant is strictly positive, one can solve ϕ_3 up to two distinct choices. Since, specifying the angles ϕ_1 and ϕ_2 completely specifies the pointing direction of the head given by (12), the two choices of ϕ_3 for a given pointing direction would correspond to two distinct orientations. The following theorem completely summarizes the picture.

Donders' Theorem III: For the angle variables ϕ_1 and ϕ_2 for which the discriminant $s^2 - 4tr > 0$ there exist precisely two distinct orientations that satisfy the Donders' constraint (19) while corresponding to the specific pointing direction (12). These two orientations are given by two distinct values of ϕ_3. On the other hand, when the discriminant $s^2 - 4\,t\,r < 0$ no orientation would satisfy both the specific heading direction (12) and the Donders' constraint (19). □

Proof of Donders' Theorem III: The unit quaternion (8) can be factored as the product

$$q(\phi_1,\phi_2,\phi_3) = \begin{pmatrix} \cos\frac{\phi_1}{2}\cos\frac{\phi_2}{2} \\ \cos\frac{\phi_1}{2}\sin\frac{\phi_2}{2} \\ \sin\frac{\phi_1}{2}\cos\frac{\phi_2}{2} \\ -\sin\frac{\phi_1}{2}\sin\frac{\phi_2}{2} \end{pmatrix} \bullet \begin{pmatrix} \cos\frac{\phi_3}{2} \\ 0 \\ 0 \\ \sin\frac{\phi_3}{2} \end{pmatrix}, \qquad (21)$$

where we recall that "$\bullet$" denotes quaternion multiplication. Let L be the composite map introduced in Proposition I, it follows from Proposition I that all preimages of $L(q(\phi_1,\phi_2,\phi_3))$ are of the form

$$\begin{pmatrix} \cos\frac{\phi_1}{2}\cos\frac{\phi_2}{2} \\ \cos\frac{\phi_1}{2}\sin\frac{\phi_2}{2} \\ \sin\frac{\phi_1}{2}\cos\frac{\phi_2}{2} \\ -\sin\frac{\phi_1}{2}\sin\frac{\phi_2}{2} \end{pmatrix} \bullet \begin{pmatrix} a \\ 0 \\ 0 \\ b \end{pmatrix}, \qquad (22)$$

where (a, b) are arbitrary points on the unit circle i.e. $a^2 + b^2 = 1$. The point of the proof of Donders' Theorem III is to ascertain how many of these quaternions satisfy the Donders' constraint (19). It would follow that the circle of quaternions would either intersect the quadratic Donders' surface at two points or no point depending upon sign of the discriminant function $s^2 - 4tr$. □

Remark V: A surprising consequence of Donders' Theorem III is that not all head pointing directions are attainable if the Donders' constraint (19) is satisfied. The unattainable pointing directions, sketched in blue, are shown in Fig. 7 for the Donders' surfaces S3, S4, S8 and S13 from [13]. □

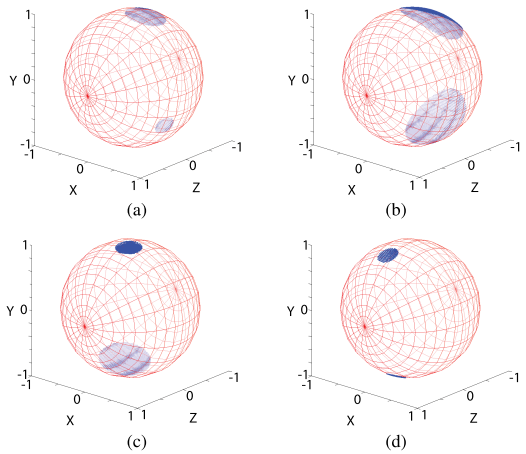

FIGURE 7. Head pointing directions for subjects with Donders surfaces sketched in [13]. Points in blue are head pointing directions that are not attainable by rotations satisfying the Donders' constraint from the primary head position. Index of the Donders' surfaces are in the captions above. The blue region of unattainable pointing directions for S2 is imperceptibly small, and is therefore not shown. (a) Data from surface S3. (b) Data from surface S4. (c) Data from surface S8. (d) Data from surface S13.

Remark VI: Carefully observing the conclusions from the two descriptions of the Donders' surfaces (15) and (19), as evidenced by the Donders' Theorems II and III, we conclude that the mapping *proj*, in (17), is $2-1$ for a large section of pointing directions[9] in S^2. In practice, this section typically includes the entire frontal pointing directions. For (15), some pointing directions have 4 preimages whereas for (19), some

[9]When the Donders' surface arises from the Fick gimbal (10), one of the two preimages of *proj*, has an orientation that correspond to the head being inverted ($\phi_3 = \pm\pi$), and is therefore physiologically unattainable.

pointing directions have no preimage. These pointing directions are typically located in the backward hemisphere, and hence they are physiologically unattainable. □

V. RIEMANNIAN METRIC AND GEODESICS

We begin our derivation of the Riemannian metric (see [43]), by assuming that the eye/head is a perfect sphere and its inertia tensor is equal to a scalar multiple[10] of the identity matrix $I_{3\times 3}$. As described in [20], one can calculate a left invariant Riemannian metric on $SO(3)$ using the isometric submersion *rot* introduced in (1). Using the axis-angle parameters from (5), the Riemannian metric on $SO(3)$ has been computed in [12] as

$$g = \begin{bmatrix} d\theta & d\phi & d\alpha \end{bmatrix} G_{AA} \begin{bmatrix} d\theta & d\phi & d\alpha \end{bmatrix}^T, \quad (23)$$

where

$$G_{AA} = \begin{pmatrix} \sin^2\frac{\phi}{2}\cos^2\alpha & 0 & 0 \\ 0 & \frac{1}{4} & 0 \\ 0 & 0 & \sin^2\frac{\phi}{2} \end{pmatrix}. \quad (24)$$

Using the Riemannian metric (23), one can write down an expression for kinetic energy KE given by

$$KE = \frac{1}{2}\left(\sin^2\frac{\phi}{2}\cos^2\alpha\,\dot{\theta}^2 + \frac{1}{4}\dot{\phi}^2 + \sin^2\frac{\phi}{2}\,\dot{\alpha}^2\right). \quad (25)$$

Using the Tait-Bryan parametrization (8), the Riemannian metric on $SO(3)$ can be written as

$$g = \begin{bmatrix} d\phi_1 & d\phi_2 & d\phi_3 \end{bmatrix} G_{TB} \begin{bmatrix} d\phi_1 & d\phi_2 & d\phi_3 \end{bmatrix}^T, \quad (26)$$

where

$$G_{TB} = \begin{pmatrix} \frac{1}{4} & 0 & -\frac{1}{4}\sin\phi_2 \\ 0 & \frac{1}{4} & 0 \\ -\frac{1}{4}\sin\phi_2 & 0 & \frac{1}{4} \end{pmatrix}. \quad (27)$$

The kinetic energy KE is easily written, analogously, as

$$KE = \frac{1}{2}\left(\frac{1}{4}\left[\dot{\phi}_1^2+\dot{\phi}_2^2+\dot{\phi}_3^2\right] - \frac{1}{2}\sin\phi_2\,\dot{\phi}_1\dot{\phi}_3\right). \quad (28)$$

Remark VII: In this remark, we would like to point out when the Riemannian Matrix G_{AA} and G_{TB} are singular. From (24) and (27) it is clear that G_{AA} is singular when $\phi = 0$ or when $\alpha = \pm\frac{\pi}{2}$. It follows from (11) that G_{AA} is singular precisely when the gaze/pointing direction is $(0\ \ 0\ \ 1)$, i.e. along the primary direction (looking/pointing straight ahead). Likewise, G_{TB} is singular when $\sin\phi_2 = \pm 1$. It follows from (12) that G_{TB} is singular precisely when the gaze/pointing direction is $(0\ \ \mp 1\ \ 0)$, i.e. looking/pointing straight down or up.[11] □

[10] We will choose this scalar multiple to be $\frac{1}{4}$.

[11] From the point of view of location of singularities, we would argue that Tait-Bryan is preferable to axis-angle parametrization.

Using the Riemannian metric (23) for $SO(3)$, the associated geodesic equation[12] is given by

$$\begin{aligned} \ddot{\theta} + \dot{\theta}\dot{\phi}\cot\tfrac{\phi}{2} - 2\dot{\theta}\dot{\alpha}\tan\alpha &= 0 \\ \ddot{\phi} - \dot{\theta}^2\sin\phi\cos^2\alpha - \dot{\alpha}^2\sin\phi &= 0 \\ \ddot{\alpha} + \tfrac{1}{2}\dot{\theta}^2\sin(2\alpha) + \dot{\phi}\dot{\alpha}\cot\tfrac{\phi}{2} &= 0. \end{aligned} \quad (29)$$

Using the Riemannian metric (26) for $SO(3)$, the associated geodesic equation is given by

$$\begin{pmatrix} \ddot{\phi}_1 \\ \ddot{\phi}_3 \end{pmatrix} = \begin{pmatrix} \tan\phi_2 & \sec\phi_2 \\ \sec\phi_2 & \tan\phi_2 \end{pmatrix} \begin{pmatrix} \dot{\phi}_1 \\ \dot{\phi}_3 \end{pmatrix} \dot{\phi}_2$$
$$\ddot{\phi}_2 = -\cos\phi_2\,\dot{\phi}_1\,\dot{\phi}_3. \quad (30)$$

Remark VIII: On the submanifold *LIST* of $SO(3)$, described by $\alpha = 0$, the Riemannian metric (23) degenerates to the form (see [20])

$$g = \begin{bmatrix} d\theta & d\phi \end{bmatrix} G_{LIST} \begin{bmatrix} d\theta & d\phi \end{bmatrix}^T, \quad (31)$$

where

$$G_{LIST} = \begin{pmatrix} \sin^2\frac{\phi}{2} & 0 \\ 0 & \frac{1}{4} \end{pmatrix}. \quad (32)$$

The corresponding geodesic equation on *LIST* is given by

$$\begin{aligned} \ddot{\theta} + \dot{\theta}\dot{\phi}\cot\tfrac{\phi}{2} &= 0 \\ \ddot{\phi} - \dot{\theta}^2\sin\phi &= 0. \end{aligned} \quad (33)$$

□

For the Riemannian metric (23), it is well known that the geodesic curves on $SO(3)$ are *great circles*. The following result from [12] is somewhat surprising.

Theorem IV (Geodesic Curve on SO(3) and LIST): Projection of the geodesic curves of $SO(3)$, that are solutions of equations (29) or (30), on the gaze/pointing space S^2, via the mapping *proj* defined in (4), is a circle. Projection of the geodesic curves of *LIST*, that are solutions of equation (33), on the gaze/pointing space S^2, via the same mapping *proj* defined in (4), is a circle that always pass through a fixed vector $(0, 0, -1)^T$. □

It will turn out that the circular shape of the geodesic curve is not retained when eye/head is modeled as an ellipsoid.

VI. DERIVATION OF ANGULAR VELOCITY

Let ω be the angular velocity of the rotating eye/head with respect to an universal coordinate (also called inertial coordinate), assumed fixed, and attached to the torso. Let q be the quaternion described in (5) and in (8). The time derivative $\dot{q}$ of q can be expressed as (see [46])

$$\dot{q} = \frac{1}{2}\,\widetilde{\omega}\bullet q, \quad (34)$$

where

$$\widetilde{\omega} = \begin{pmatrix} 0 \\ \omega \end{pmatrix}$$

[12] Geodesic equations were computed in [20] using *Christoffel symbols* [44] and *Connection* [45].

$$M_{AA} = \begin{pmatrix} -\cos\alpha\,(2\cos\theta\sin\alpha\sin^2\frac{\phi}{2}+\sin\theta\sin\phi) & \cos\alpha\,\cos\theta & (1-\cos\phi)\sin\theta-\cos\theta\sin\alpha\sin\phi \\ -\sin(2\alpha)\sin\theta\sin^2\frac{\phi}{2}+\cos\alpha\cos\theta\sin\phi & \cos\alpha\,\sin\theta & \cos\theta(\cos\phi-1)-\sin\alpha\,\sin\theta\,\sin\phi \\ 2\cos^2\alpha\,\sin^2\frac{\phi}{2} & \sin\alpha & \cos\alpha\,\sin\phi \end{pmatrix}. \quad (36)$$

$$G_{LIST} = \begin{pmatrix} [m_1+m_2+2m_3+(m_1+m_2-2m_3)\cos(3\phi)+(m_2-m_1)\cos(2\theta)(1+\cos(3\phi))]\sin^2\frac{\phi}{2} & \frac{(m_2-m_1)}{2}(2\cos\phi-1)\sin(2\theta)\,\sin\phi \\ \frac{(m_2-m_1)}{2}(2\cos\phi-1)\sin(2\theta)\,\sin\phi & \frac{1}{2}(m_1+m_2+(m_1-m_2)\cos(2\theta)) \end{pmatrix} (42)$$

is a quaternion whose vector part is the angular velocity ω. Using (5), (8) and (34), one can explicitly compute the vector ω in terms of the axis-angle or Tait-Bryan parameters in the following form

$$\omega = M\,\dot{\Theta}, \quad (35)$$

where M is a 3×3 matrix. In the axis-angle parameters

$$\Theta = (\theta,\phi,\alpha)^T$$

the matrix M_{AA} is given by (36), as shown at the top of this page. In the Tait-Bryan parameters

$$\Theta = (\phi_1,\phi_2,\phi_3)^T \quad (37)$$

the matrix

$$M_{TB} = \begin{pmatrix} 0 & \cos\phi_1 & \cos\phi_2\sin\phi_1 \\ 1 & 0 & -\sin\phi_2 \\ 0 & -\sin\phi_1 & \cos\phi_1\cos\phi_2 \end{pmatrix}.$$

A simple algebraic manipulation shows that

$$G_{AA} = \frac{1}{4}M_{AA}^T M_{AA}, \quad (38)$$

and

$$G_{TB} = \frac{1}{4}M_{TB}^T M_{TB}. \quad (39)$$

Choosing the moment of inertia to be $\frac{1}{4}I_{3\times 3}$, where $I_{3\times 3}$ is a 3 by 3 identity matrix, we compute that the kinetic energy

$$KE = \frac{1}{2}\left(\omega^T\left(\frac{1}{4}I_{3\times 3}\right)\omega\right)$$

matches precisely the definition chosen earlier in (25) and (28).

Remark IX: When the moment of inertia is an arbitrary symmetric, positive definite matrix J (in the body coordinate), we define kinetic energy given by

$$KE = \frac{1}{2}\left(\omega^T\,\bar{J}\,\omega\right) = \frac{1}{2}\left(\dot{\Theta}^T\,\left(M^T\,\bar{J}\,M\right)\,\dot{\Theta}\right),$$

where

$$\bar{J} = Q^T\,J\,Q, \quad (40)$$

is moment of inertia in the inertial coordinate, and where Q has been defined in (3). If we define the Riemannian matrix as

$$G_{AA} = M_{AA}^T\,\bar{J}\,M_{AA}\ \ and\ \ G_{TB} = M_{TB}^T\,\bar{J}\,M_{TB}, \quad (41)$$

we obtain Riemannian metric analogous to (23) and (26). □

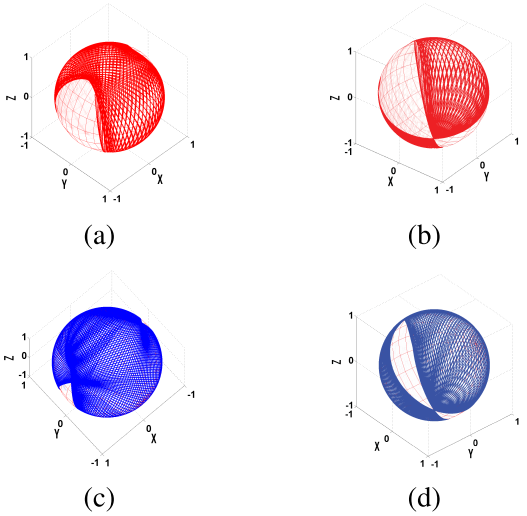

FIGURE 8. A geodesic curve from a typical human eye projected on the gaze space, under Listing's constraint. The moment of inertia is constructed from the parameters of a typical human eye and has been chosen as $m_1 = 1.0211$, $m_2 = 1.0000$, $m_3 = 1.0417$. The parameters have been normalized making the smallest m_i to be 1. (a) Projection of a single geodesic curve on *LIST* in the gaze space using axis-angle parametrization. The initial conditions are $\theta = \frac{\pi}{8}$, $\dot{\theta} = 1$, $\phi = \frac{\pi}{4}$, $\dot{\phi} = 2$. The figure shows the front view. (b) The figure shows the back view of the geodesic curve in Fig. 8a. Note that the curve passes through the backward gaze point repeatedly. (c) Projection of a geodesic curve on *LIST* in the gaze space using axis-angle parametrization. The initial conditions are $\theta = \frac{\pi}{16}$, $\dot{\theta} = 1$, $\phi = \frac{\pi}{8}$, $\dot{\phi} = 3$. (d) The figure shows the back view of the geodesic curve in Fig. 8c. Note that the curve passes through the backward gaze point repeatedly.

Remark X: When $J = diag(m_1,m_2,m_3)$, the determinants of the Riemannian matrices G_{TB} and G_{AA} from (41) are obtained as

$$det(G_{TB}) = m_1m_2m_3\cos^2\phi_2,$$

and

$$det(G_{AA}) = 16\,m_1m_2m_3\cos^2\alpha\,\sin^4\frac{\phi}{2}.$$

These determinants do not change even when the moment of inertia of the body is an arbitrary symmetric, positive definite matrix J. It follows that the singularities of G_{TB} and G_{AA} are precisely as was described in Remark VII. Likewise, one can define G_{LIST} as

$$G_{LIST} = M_{LIST}^T\,\bar{J}\,M_{LIST},$$

where M_{LIST} is the first two columns of the matrix M_{AA} in (36). The matrix G_{LIST}[13] is given by (42), as shown at the top of the page. and we compute

$$det(G_{LIST}) = 4m_3(m_1\cos^2\theta + m_2\sin^2\theta)\sin^4\frac{\phi}{2} + m_1m_2\sin^2\phi,$$

so that G_{LIST} is singular precisely when $\phi = 0$, i.e. when the gaze/pointing direction is *looking straight ahead*. The main point of this remark is to verify that the structure of the matrix J does not move the singular points of the corresponding Riemannian matrix G. □

VII. CONTROLLED LAGRANGIAN DYNAMICS AND EULER-LAGRANGE'S EQUATION

We describe the eye and head rotation as a Lagrangian dynamics [47], where the dynamics is described using a Lagrangian L where

$$L = KE - PE, \tag{43}$$

and the corresponding Euler-Lagrange's equation

$$\frac{d}{dt}\left(\frac{\partial L}{\partial \dot\beta}\right) - \left(\frac{\partial L}{\partial \beta}\right) = \tau_\beta. \tag{44}$$

The kinetic energy functions (KE) are already introduced in sections V and VI. The movement dynamics is additionally affected by a potential energy term PE[14] and an externally applied input (τ_β), where β represents the angle variables θ, ϕ, α for the axis-angle parametrization and ϕ_1, ϕ_2, ϕ_3 for the Tait-Bryan parametrization. The notation τ_β is for the generalized torque. Let

$$T = (T_1,\ T_2,\ T_3)^T,$$

be the external torque applied to the eye or head, represented in the inertial coordinate referred to in section VI, we remark that the generalized torque vector $\tau = (\tau_\theta, \tau_\phi, \tau_\alpha)^T$ is related to T by a transformation described as

$$\tau = M^T\,T \tag{45}$$

where M has been defined in (35). From (45), we obtain the following[15]

$$\|T\|^2 = \tau^T\,(M^TM)^{-1}\,\tau. \tag{46}$$

The right hand side of (46) evaluates to

$$\frac{1}{4}\sec^2\alpha\,\csc^2\frac{\phi}{2}\,\tau_\theta^2 + \tau_\phi^2 + \frac{1}{4}\csc^2\frac{\phi}{2}\,\tau_\alpha^2. \tag{47}$$

for the axis-angle parameters. In the Tait-Bryan parametrization, the corresponding right hand side of (46) is given by

$$\sec^2\phi_2\,\tau_{\phi_1}^2 + \tau_{\phi_2}^2 + \sec^2\phi_2\,\tau_{\phi_3}^2 + 2\sin\phi_2\sec^2\phi_2\,\tau_{\phi_1}\tau_{\phi_3} \tag{48}$$

[13]The matrices (32) and (42) should be compared, and one should note that when J is not a multiple of the identity matrix, the diagonal structure of the G matrix is lost. This makes the problem of computing optimal controllers for ellipsoidal bodies, much harder.

[14]Throughout this paper, the potential energy term is assumed to be absent. It is added only in the appendix X, where we introduce potential based control.

[15]The notation $\|\cdot\|$ is the standard Euclidean norm.

We finish this section by writing the description of the Euler-Lagrange equation (44), for specific parameterizations on $SO(3)$ and $LIST$ considered in equations (29), (30) and (33). We continue to assume that the potential function PE in (43) is identically 0. Attaching the term $G^{-1}\tau$ to the right hand sides of (29), (30) and (33), we obtain

$$\begin{aligned}
\ddot\theta + \dot\theta\dot\phi\cot\tfrac{\phi}{2} - 2\dot\theta\dot\alpha\tan\alpha &= \sec^2\alpha\csc^2\tfrac{\phi}{2}\tau_\theta\\
\ddot\phi - \dot\theta^2\sin\phi\cos^2\alpha - \dot\alpha^2\sin\phi &= 4\tau_\phi\\
\ddot\alpha + \tfrac{1}{2}\dot\theta^2\sin(2\alpha) + \dot\phi\dot\alpha\cot\tfrac{\phi}{2} &= \csc^2\tfrac{\phi}{2}\tau_\alpha.
\end{aligned} \tag{49}$$

on $SO(3)$ using axis-angle parametrization;

$$\begin{aligned}
\begin{pmatrix}\ddot\phi_1\\ \ddot\phi_3\end{pmatrix} &= \begin{pmatrix}\tan\phi_2 & \sec\phi_2\\ \sec\phi_2 & \tan\phi_2\end{pmatrix}\begin{pmatrix}\dot\phi_1\\ \dot\phi_3\end{pmatrix}\dot\phi_2\\
&\quad + 4\sec^2\phi_2\begin{pmatrix}1 & \sin\phi_2\\ \sin\phi_2 & 1\end{pmatrix}\begin{pmatrix}\tau_{\phi_1}\\ \tau_{\phi_3}\end{pmatrix}\\
\ddot\phi_2 &= -\cos\phi_2\,\dot\phi_1\,\dot\phi_3 + 4\,\tau_{\phi_2}.
\end{aligned} \tag{50}$$

on $SO(3)$ using Tait-Bryan parametrization; and

$$\begin{aligned}
\ddot\theta + \dot\theta\dot\phi\cot\frac{\phi}{2} &= \csc^2\frac{\phi}{2}\,\tau_\theta\\
\ddot\phi - \dot\theta^2\sin\phi &= 4\,\tau_\phi.
\end{aligned} \tag{51}$$

on $LIST$ using axis angle parametrization. The equations (49) and (51) were already introduced in [12]. The equation (50) is new.

Remark XI: The Euler-Lagrange equation (44) can be written in a compact form (see [13]) as

$$G\ddot\Theta + \dot G\dot\Theta - \nabla_\Theta L = \tau, \tag{52}$$

where G is the Riemannian matrix, L is the Lagrangian (43), $\Theta = (\theta_1, \theta_2, \theta_3)$ is the parameter vector[16] and τ is the vector of generalized torques. Finally, we define ∇_Θ is the gradient operator with respect to Θ defined as

$$\nabla_\Theta = \left(\frac{\partial}{\partial\theta_1}, \frac{\partial}{\partial\theta_2}, \frac{\partial}{\partial\theta_3}\right)^T. \tag{53}$$

When J is an arbitrary symmetric, positive definite matrix, we can use the definition of G in (41) to write the Euler-Lagrange's equation using (52). □

VIII. CONTROLLED RICCATI DYNAMICS

The approach that we had been using so far in this paper, to describe a rigid body dynamics, is to either use axis-angle or the Tait-Bryan parameters. In this section, instead of using the Euler-Lagrange equation, we propose to use Newton-Euler formulation of the dynamics [35]. We begin with a discussion, which is perhaps quite standard (see [3]).

Let us start with a fixed inertial coordinate frame, denoted by e. A rigid body is rotating with respect to the frame e and we assume that a frame b is attached to the body (called the body frame). Let x and x_b be coordinates of a vector with

[16]For $LIST$ the parameter vector is 2 dimensional and the definition of ∇_X in (53) has to be adjusted accordingly. On $SO(3)$, Θ is either (θ, ϕ, α) for axis-angle or (ϕ_1, ϕ_2, ϕ_3) for Tait-Bryan parameters.

respect to frames e and b, respectively, it follows that the coordinates are related by

$$x_b \;=\; Q\,x,$$

where Q is the rotation matrix introduced in (3). Let J be a constant moment of inertia matrix of the rigid body in the body frame, and let ω_b be the angular velocity vector in the body frame b. Finally let T_b be the expression of the external torque in the body frame, we have the following, well known, dynamic equation

$$J\,\dot{\omega}_b(t) \;=\; -\omega_b(t)\times(J\omega_b(t)) \;+\; T_b(t). \tag{54}$$

A simple algebraic manipulation yields the following description of the dynamic equation in the inertial coordinates

$$\bar{J}(t)\,\dot{\omega}(t) \;=\; -\omega(t)\times(\bar{J}(t)\,\omega(t)) \;+\; T(t), \tag{55}$$

where $\bar{J}(t)$ has been defined (40) in remark IX, and note that $T(t)$ is the external torque in the inertial frame. Note also that ω is the angular velocity vector in the inertial frame, as was introduced earlier in (35).

Remark XII: For a rigid body, the matrix J is a constant but the matrix $\bar{J}(t)$ is not. It would therefore appear that the equation (54) is simpler to use compared to (55). In this paper, however, we use the latter equation. This is because, in the equation (34), the angular velocity vector ω is defined in the inertial frame. □

Rewriting (34) as

$$\frac{d}{dt}\begin{bmatrix} q_0\\ q_1\\ q_2\\ q_3\end{bmatrix} \;=\; \frac{1}{2}\begin{pmatrix} 0\\ \omega_1\\ \omega_2\\ \omega_3\end{pmatrix}\bullet\begin{bmatrix} q_0\\ q_1\\ q_2\\ q_3\end{bmatrix}, \tag{56}$$

where we recall that $\bullet$ is *quaternion multiplication*. The equation (56) is to be viewed as an equation on the projective space $\mathbf{P}^3$ [48], [49]. When $q_0 \neq 0$, we define coordinates on the projective space given by

$$\bar{q}_i \;=\; \frac{q_i}{q_0}, \quad \text{for } i=1,2,3.$$

In these coordinates, the dynamics (56) can be written as

$$2\begin{pmatrix}\dot{\bar{q}}_1\\ \dot{\bar{q}}_2\\ \dot{\bar{q}}_3\end{pmatrix} = \begin{pmatrix}\omega_1\\ \omega_2\\ \omega_3\end{pmatrix} + \begin{pmatrix} 0 & -\omega_3 & \omega_2\\ \omega_3 & 0 & -\omega_1\\ -\omega_2 & \omega_1 & 0\end{pmatrix}\begin{pmatrix}\bar{q}_1\\ \bar{q}_2\\ \bar{q}_3\end{pmatrix}$$
$$+\begin{pmatrix} \omega_1 & 0 & 0 & 0 & \omega_3 & \omega_2\\ 0 & \omega_2 & 0 & \omega_3 & 0 & \omega_1\\ 0 & 0 & \omega_3 & \omega_2 & \omega_1 & 0\end{pmatrix}\begin{pmatrix}\bar{q}_1^2\\ \bar{q}_2^2\\ \bar{q}_3^2\\ \bar{q}_2\bar{q}_3\\ \bar{q}_1\bar{q}_3\\ \bar{q}_1\bar{q}_2\end{pmatrix}. \tag{57}$$

The dynamical system (57) is the Riccati Dynamics [50], corresponding to the homogeneous system (56) (see [51] for Riccati connection to homogeneous systems). The pair of equations (55), (57) describe a controlled Riccati equation. The control is given by external torque vector $T(t)$ on the eye/head represented in the inertial coordinates.

Remark XIII: When the moment of inertia matrix $J = \frac{1}{4}I_{3\times 3}$, where $I_{3\times 3}$ is the identity matrix, the equation (55) reduces to

$$\dot{\omega}(t) \;=\; 4T(t). \tag{58}$$

Substituting the description of ω in terms of the derivative of the angle parameters from (35) we write

$$\dot{\omega}(t) \;=\; M\,\ddot{\Theta} \;+\; \dot{M}\,\dot{\Theta}. \tag{59}$$

Combining, (58) and (59) we obtain

$$\ddot{\Theta} \;+\; M^{-1}\dot{M}\,\dot{\Theta} \;=\; 4M^{-1}\,T(t), \tag{60}$$

which is an alternative description of the Euler-Lagrange's equations (49) and (50) (see also (52)). Multiplying (52) by G^{-1} and equating the right hand side with the right hand side of (60) we obtain

$$T(t) \;=\; \frac{1}{4}M\,G^{-1}\,\tau(t). \tag{61}$$

Since G is $\frac{1}{4}M^TM$, we recover (45) from (61).

When the moment of inertia matrix J is an arbitrary symmetric, positive definite matrix, the calculations made in this remark can be repeated and we can recover (45) as well. □

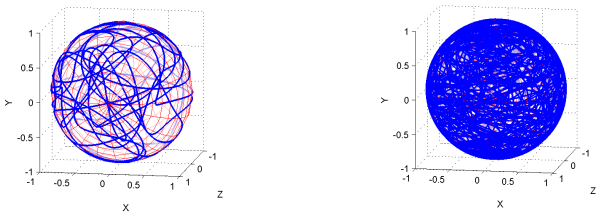

(a) (b)

FIGURE 9. Geodesic pointing directions from a human head of ellipsoidal shape rotating about the south pole. The moment of inertia matrix, in body coordinates, is *diag*(.2718, .0529, .2698) in $kg\,m^2$ units. The initial conditions are at $\phi_1 = \phi_2 = \phi_3 = 0$, and $\dot{\phi}_1 = \dot{\phi}_2 = \dot{\phi}_3 = 5$. (a) Using Tait-Bryan parametrization, the geodesic curve on $SO(3)$ has been projected onto the pointing space S^2. Simulation time is 10 secs. (b) Geodesic curve on $SO(3)$ projected on S^2 as on the left, where the simulation time is continued for 100 secs.

IX. EXAMPLES OF OPTIMAL CONTROL PROBLEM

The optimal control problems we discuss here are introduced in greater details in [4]. Typically, our interest is to rotate the human eye or the head from one gaze/pointing direction to another, in a finite time interval which we assume to be $[0, 1]$. We therefore assume that the state variables Θ and $\dot{\Theta}$ have prescribed values[17] at $t = 0$ and at $t = 1$.

[17]Typically one could assume that $\dot{\Theta}(0) = \dot{\Theta}(1) = 0$.

There are of course multiple ways to steer the eye/head between the two gaze/pointing directions, and our goal is to achieve this objective[18] with minimum cost, as measured by a cost function.

Recall from (52) that we can write the Euler Lagrange's equation as

$$\ddot{\Theta} \;=\; F, \tag{62}$$

where

$$F \;=\; G^{-1}\left[\tau \;-\; \dot{G}\,\dot{\Theta} \;+\; \nabla_{\Theta} L\right].$$

For both eye and head, one of our goal is to calculate an optimal generalized torque vector τ that minimizes a cost function in the form

$$CF \;=\; \int_0^1 \frac{\delta}{2}\,\|T\|^2, \tag{63}$$

where $\|T\|^2$ has been computed in (46), and δ is a constant weight. One way to compute the optimal control is to augment the dynamics (62) as a part of the cost function (63) and write

$$CF \;=\; \int_0^1 \frac{\delta}{2}\,\|T\|^2 \;+\; p(t)^T\,\left(F \;-\; \ddot{\Theta}\right)\,dt. \tag{64}$$

The variable $p(t)$ is the *Lagrange-Multiplier* and is called the costate variable in this context. We define

$$H \;=\; \frac{\delta}{2}\,\tau^T\,Z(\Theta)\,\tau \;+\; p^T F,$$

where $Z(\Theta) = (M^T M)^{-1}$ and rewrite (64) as

$$CF \;=\; \int_0^1 (H \;-\; p^T\ddot{\Theta})\,dt. \tag{65}$$

A necessary condition for optimal control is obtained by taking the variation [52] of (65) with respect to Θ, p and τ and setting the result to zero. We obtain

$$\ddot{\Theta} \;=\; \frac{\partial H}{\partial p} \;=\; F;\;\; \ddot{p} \;=\; \frac{\partial H}{\partial \Theta} \;-\; \frac{d}{dt}\left(\frac{\partial H}{\partial \dot{\Theta}}\right). \tag{66}$$

The optimal control τ is obtained as

$$\tau \;=\; -\frac{1}{\delta}\,(GZ)^{-1}p.$$

The equation (66) is called the Hamiltonian-Equation and the function H is called the Hamilton's function. Note in particular that when $J = \frac{1}{4}I_{3\times 3}$, then the optimal generalized torque control τ takes a simple form given by

$$\tau \;=\; -\frac{4}{\delta}\,p. \tag{67}$$

The states of the equation (66) are Θ, $\dot{\Theta}$, p, $\dot{p}$, and typically we are given initial and final values $\Theta(0)$, $\dot{\Theta}(0)$, $\Theta(1)$, $\dot{\Theta}(1)$.

Remark XIV: From the point of view of eye and head rotations, often we are interested in restricting the state Θ to a submanifold of $SO(3)$, such as *LIST* or *DOND*. We define the constrained space as

$$D(\Theta) \;=\; 0.$$

In this case, we modify the function H as

$$\bar{H} \;=\; \frac{\delta}{2}\,\tau^T\,Z(\Theta)\,\tau \;+\; p^T F \;+\; \lambda\,D,$$

where $\lambda(t)$ is another *Lagrange-Multiplier*. The cost function CF is now written as

$$CF \;=\; \int_0^1 (\bar{H} \;-\; p^T\ddot{\Theta}) + \frac{\varepsilon}{2}\,\dot{\lambda}^2\,dt, \tag{68}$$

where the last term is a penalty term, that has been added to make λ smooth. We obtain an equation similar to (66) as follows

$$\ddot{\Theta} \;=\; \frac{\partial \bar{H}}{\partial p} \;=\; F;\;\; \ddot{p} \;=\; \frac{\partial \bar{H}}{\partial \Theta} \;-\; \frac{d}{dt}\left(\frac{\partial \bar{H}}{\partial \dot{\Theta}}\right);\;\; \ddot{\lambda} \;=\; \frac{1}{\varepsilon}\,D(\Theta). \tag{69}$$

The optimal control is still given by (67). □

We now sketch some specific examples of the optimal control problem.

A. OPTIMAL CONTROL USING AXIS-ANGLE PARAMETERS

Using the axis-angle parametrization, we start by looking at the dynamical system (49). Our goal is a synthesize an optimal controller that minimizes a cost function in the form

$$\frac{\delta}{2}\int_0^1 \|T(t)\|^2 dt \;=\; \frac{\delta}{2}\int_0^1 \frac{1}{4}\sec^2\alpha\,\csc^2\frac{\phi}{2}\,\tau_\theta^2 \;+\; \tau_\phi^2 \;+\; \frac{1}{4}\csc^2\frac{\phi}{2}\,\tau_\alpha^2\;dt. \tag{70}$$

Recall that the cost function originally considered in [13] is

$$\frac{\delta}{2}\int_0^1 \|\tau(t)\|^2 dt \;=\; \frac{\delta}{2}\int_0^1 \tau_\theta^2(t) + \tau_\phi^2(t) + \tau_\alpha^2(t)\;dt, \tag{71}$$

where τ is the vector of generalized torque. We now restrict the state space to satisfy Listing's constraint $\alpha = 0$, by defining $D(\Theta) = \alpha$. In Fig. 10, the corresponding optimal trajectory has been plotted. In comparing the two cost functions (71) and (70), we would like to remark that perhaps minimizing (70) is more practical and reasonable, since it minimizes the magnitude of the external torque. On the other hand, the cost function (71) was used in [12]. Fig. 10 shows that the optimal trajectories, for the two cost functions, are close although generalized torques produce trajectories of shorter length.

B. OPTIMAL CONTROL USING TAIT-BRYAN PARAMETERS

As is subsection IX-A, we are now looking at the dynamical system (50), together with a cost function in the form

$$\frac{\delta}{2}\int_0^1 \|T(t)\|^2 dt = \frac{\delta}{2}\int_0^1 \sec^2\phi_2 \times\left[\tau_{\phi_1}^2(t) + \tau_{\phi_3}^2(t) + 2\sin\phi_2\,\tau_{\phi_1}\tau_{\phi_3}\right] + \tau_{\phi_2}^2(t)\;dt. \tag{72}$$

[18] It has been argued in [4] that other objectives, such as tracking a prescribed trajectory, are important as well, for example in Eye/Head coordination.

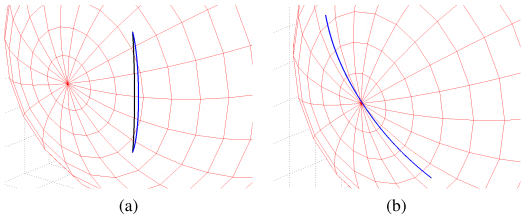

FIGURE 10. Sphere rotating about center satisfying Listing's constraint. The center of the circle in the above two figures shows frontal gaze direction. The black curve is when the cost function (71), minimizes the vector of generalized torque τ. The blue curve is when the cost function (70), minimizes the vector of external torque T. In Fig. 10b, the black and blue curves cannot be seen separately. (a) The eye moves from left/bottom to left/top. The initial conditions are $\theta(0) = \frac{\pi}{4}$, $\phi(0) = \frac{\pi}{6}$, $\alpha(0) = 0$, $\dot{\theta}(0) = \dot{\phi}(0) = \dot{\alpha}(0) = 0$. The final conditions are $\theta(1) = \frac{3\pi}{4}$, $\phi(1) = \frac{\pi}{6}$, $\alpha(1) = 0$, $\dot{\theta}(1) = \dot{\phi}(1) = \dot{\alpha}(1) = 0$. (b) The eye moves from left/bottom to right/top. The initial conditions are $\theta(0) = \frac{\pi}{4}$, $\phi(0) = \frac{\pi}{6}$, $\alpha(0) = 0$, $\dot{\theta}(0) = \dot{\phi}(0) = \dot{\alpha}(0) = 0$. The final conditions are $\theta(1) = \frac{5\pi}{4}$, $\phi(1) = \frac{\pi}{6}$, $\alpha(1) = 0$, $\dot{\theta}(1) = \dot{\phi}(1) = \dot{\alpha}(1) = 0$.

We compare our optimal trajectories with the one obtained using cost function in the form

$$\frac{\delta}{2}\int_0^1 \tau_{\phi_1}^2(t) + \tau_{\phi_2}^2(t) + \tau_{\phi_3}^2(t)\, dt, \tag{73}$$

considered in [13]. The optimal trajectories are sketched in Fig. 11, assuming that the states are restricted to satisfy Donders' constraint. We have used Donders' surface S2 from surface 2 in [13] and from the Fick gimbals.[19] We have used the cost function (72) in Fig. 11a and the cost function (73) in Fig. 11b. We note, once again, that generalized torques produce trajectories of shorter length.

C. OPTIMAL CONTROL USING CONTROLLED RICCATI DYNAMICS

In this section, we would like to refer back to the Riccati dynamics (57) from section VIII. We also consider the dynamics of the angular velocity vector ω given by (58). We would like to optimally regulate the eye movement while minimizing the cost function (63). As in (64), we augment the cost function by considering a new cost function given by

$$\begin{aligned} CF \;=\; & \int_0^1 \tfrac{\delta}{2}\,\left(T_1^2+T_2^2+T_3^2\right) \\ & +\; p_1\left[\tfrac{1}{2}\left(\omega_1+\bar{q}_3\omega_2-\bar{q}_2\omega_3+\bar{q}_1^2\omega_1+\bar{q}_1\bar{q}_2\omega_2+\bar{q}_1\bar{q}_3\omega_3\right)-\dot{\bar{q}}_1\right] \\ & +\; p_2\left[\tfrac{1}{2}\left(\omega_2+\bar{q}_1\omega_3-\bar{q}_3\omega_1+\bar{q}_2^2\omega_2+\bar{q}_1\bar{q}_2\omega_1+\bar{q}_2\bar{q}_3\omega_3\right)-\dot{\bar{q}}_2\right] \\ & +\; p_3\left[\tfrac{1}{2}\left(\omega_3+\bar{q}_2\omega_1-\bar{q}_1\omega_2+\bar{q}_3^2\omega_3+\bar{q}_1\bar{q}_3\omega_1+\bar{q}_2\bar{q}_3\omega_2\right)-\dot{\bar{q}}_3\right] \\ & +\; p_4\left[T_1-\dot{\omega}_1\right]+p_5\left[T_2-\dot{\omega}_2\right]+p_6\left[T_3-\dot{\omega}_3\right]\, dt. \end{aligned} \tag{74}$$

Additionally, if the state variable is to be restricted to the Listing's plane, $\bar{q}_3 = 0$, we further augment the cost function (74) with the Listing's constraint and obtain the following

$$CF_{LIST} \;=\; CF \;+\; \int_0^1 \lambda\bar{q}_3 + \frac{\varepsilon}{2}\dot{\lambda}^2\, dt. \tag{75}$$

[19]Donders' surface arising from Fick gimbals is given by $\phi_3 = 0$. Donders' surface S2 is described in the form (20).

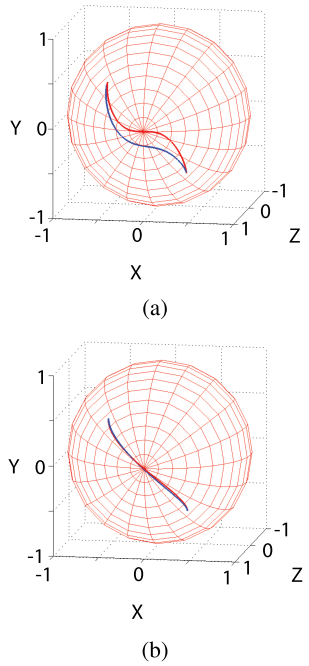

FIGURE 11. Optimal control of a sphere rotating about center. In blue curve, the Donders' surface is chosen as S2, from surface 2 in [13]. The red curve is when the Donders' surface is from Fick gimbal. Initial and final conditions of the angle ϕ_3 is calculated using the Donders' surface. (a) The initial condition is $\phi_1(0) = \phi_2(0) = \frac{\pi}{6}$, $\dot{\phi}_1(0) = \dot{\phi}_2(0) = \dot{\phi}_3(0) = 0$. The final condition is $\phi_1(1) = \phi_2(1) = -\frac{\pi}{6}$, $\dot{\phi}_1(1) = \dot{\phi}_2(1) = \dot{\phi}_3(1) = 0$. The cost function minimizes the magnitude of the external torque T in inertial coordinates. (b) The initial condition is $\phi_1(0) = \phi_2(0) = -\frac{\pi}{6}$, $\dot{\phi}_1(0) = \dot{\phi}_2(0) = \dot{\phi}_3(0) = 0$. The final condition is $\phi_1(1) = \phi_2(1) = -\frac{\pi}{6}$, $\dot{\phi}_1(1) = \dot{\phi}_2(1) = \dot{\phi}_3(1) = 0$. The cost function minimizes the magnitude of the generalized torque τ.

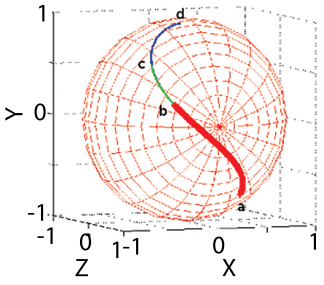

FIGURE 12. Projection of the solution to the Euler-Lagrange's equation (81), assuming potential energy PE is zero, has been plotted starting from the head pointing direction a. For $c = 0$, in (79), the projection of the geodesic is plotted as a blue curve from a to d. For $c = 0.25$ the projection of the solution is plotted as a green curve from a to c. Finally for $c = 0.50$ the projection is plotted as a red curve from a to b. The figure demonstrates that all curves trace out a portion of the geodesic.

As commented in remark XIV, the variable λ is another Lagrange's multiplier and the last term in (75) is a penalty term, added in order to make λ smooth. Lastly, if the state variable is to be restricted to the Donders' surface arising from the Fick gimbal, $\bar{q}_3 + \bar{q}_1\,\bar{q}_2 = 0$, we further augment the cost function (74) with the corresponding Donders' constraint and obtain the following

$$CF_{FICK} \;=\; CF \;+\; \int_0^1 \lambda\left[\bar{q}_3+\bar{q}_1\,\bar{q}_2\right]+\frac{\varepsilon}{2}\dot{\lambda}^2\, dt. \tag{76}$$

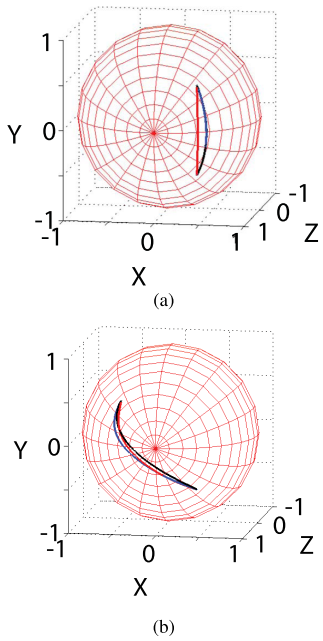

FIGURE 13. Simulations of the human head being potentially controlled. The figures show movement of the head on the pointing space. In the caption above, S2 is used to mean the Donders' surface from surface 2 in [13]. Blue curve is the trajectory of a typical human head, satisfying Donders' surface S2 (see Fig. 5a). Black curve is same as the blue curve except that the human head is replaced by a sphere. Finally the red curve is same as the blue curve except that the Donders' surface is replaced by *Fick gimbal*. All rotations are about the south pole (neck). (a) The initial conditions are $\phi_1 = \frac{\pi}{6}, \phi_2 = \frac{\pi}{6}$. The final conditions are $\phi_1 = \frac{\pi}{6}, \phi_2 = -\frac{\pi}{6}$. The angle ϕ_3 is calculated using the Donders' surface. The blue and the black curves are overlapping. (b) The initial conditions are $\phi_1 = \frac{\pi}{6}$, $\phi_2 = \frac{\pi}{6}$. The final conditions are $\phi_1 = -\frac{\pi}{6}, \phi_2 = -\frac{\pi}{6}$. The angle ϕ_3 is calculated using the Donders' surface.

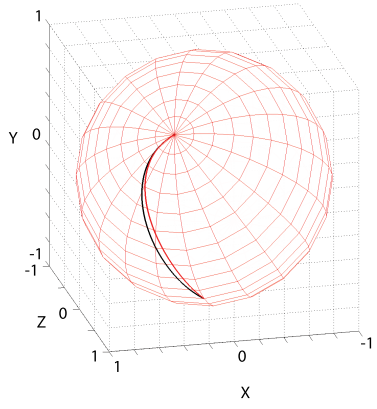

FIGURE 14. Sphere rotating about center. Optimal curve joining the gaze/pointing directions $(0, 0, 1)^T$ (frontal gaze direction, shown as north pole) and $(0, -1, 0)^T$ (gaze direction looking straight down). The former is a singular point of axis-angle parametrization and the latter is a singular point of Tait-Bryan parametrization. In this simulation, we have used the q parametrization. The initial and the final conditions on $\dot{\bar{q}}_i$ are zero for $i = 1, 2, 3$. Black color is when state is restricted by Listing's constraint. Red color is when state is restricted by Donders' surface arising from Fick gimbal.

The optimal control is synthesized by taking variation with respect to vectors $\bar{q}$, ω, p and T and λ. In Fig. 14, the optimal trajectories have been plotted when the body is made to move between two gaze/pointing directions assuming that the state

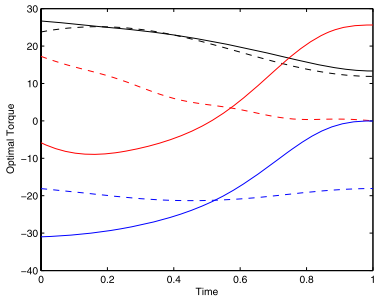

FIGURE 15. Optimal torques from Fig. 14. Dashed lines are when the state is constrained by Listing. Continuous lines are when the state is constrained by Fick gimbal. Black, Blue and Red shows T_1, T_2 and T_3 respectively. It is interesting to note that although the torque profiles in this figure are substantially different, the optimal trajectories in Fig. 14 are close.

is constrained by Listing's (respectively Fick) constraint. The end points are deliberately chosen as points where either the dynamical system using axis-angle or the Tait-Bryan parameters hit a singularity. Simulation shows that although the optimal trajectories in Fig. 14 are 'close', the optimal torque functions (shown in Fig. 15) are not.

X. CONCLUSION

A geometric approach to controlling eye and head movement is introduced in this paper, even when the eye and the head are not perfect spheres and when the head is not rotating about its center. Taking parameters from a typical human adult, eye and head geodesic trajectories have been simulated and their projections on the gaze/pointing space have been plotted. Furthermore, choosing the same parameters, and assuming that the Donders' surface is borrowed from one of the six human subjects reported in [13], we have plotted the potentially controlled trajectories. These trajectories are compared under a more relaxed assumption when the Donders' surface comes from a simplified *Fick gimbal* and when the head is replaced by a perfect sphere. It is interesting to observe that the non-spherical shape did not affect the trajectories appreciably.

The paper also introduces a non-Lagrangian approach to solving optimal control problems by writing a *Riccati dynamics* on S^3, where the control torque affects the angular velocity vector. In this, so called Newton-Euler formulation, the dynamical system (57) does not have a singularity. However, the variables $\bar{q}_i$, $i = 1, 2, 3$ are not defined when $q_0 = 0$, i.e. when $\phi = \pi$, equivalently when the gaze/pointing direction is backwards. Additionally, an obvious disadvantage is the lack of a suitable *potential control approach*. Although muscle models are not discussed in this paper, they have been introduced in [20] using a Lagrangian formulation of the dynamics.

As a final remark, we would like to point out the following partial list of application areas where we think this paper will make contact in the future.

- **Gaze Stabilization Therapy:** All animals are confronted with the problem of stabilizing gaze in spite of disruptive effects of locomotory action [53]. For

humans, the head and body movements are to be compensated by an opposite movement of the eye [4]. It is believed that the compensatory eye movement is implemented by vestibular error sensory feedback. Vestibular signals also play a role in motor learning over repeated trials, using an efference copy signalling [54]. Modeling and optimal control problems in the gaze stabilizing circuit of patients with chronic bilateral vestibular loss, would be important for their therapy (see [55]).

- **Motion Parallax in Humanoid Robotics:** Motion parallax is the displacement in the retinal position of the projection of an object as an animal moves through the environment [56]. It has been reported in owls, insects, birds and mammals [57], [58], that parallax resulting from head and eye movements contain depth information that can compliment stereopsis techniques well-known in Robotics [59], [60]. The motion models presented in this paper can be extended to estimate motion parallax, with possible application to humanoid robots [61].
- **Multi-Ocular Vision in Human Robot Team:** Human vision is binocular [15], yet it is unclear how two eyes are controlled simultaneously to focus between targets (see [62]). A well known principle for binocular control is due to Hering [63], wherein it has been proposed that the control action on the two eyes can be decomposed into *version* and *vergence* components (see [64], [65]). The motion models of eye and head rotations, presented in this paper, can be used to study binocular control, and to teams of vehicles equipped with visual capabilities (that include human and robot vision). A possible scenario for control action is to orient vehicles and the visual sensors, to maximize motion parallax (as described above). The control action can also be to minimize motion parallax (also called motion camouflage) in 3D, possibly with a team of agents [66] equipped with orientable vision sensors. Such problems, arising from predator/prey dynamics in Biology, are of military interest as well [67].
- **Wearable Electrooculography in Video Games:** Human activities, such as reading or driving, can be recognized from eye movement activities [68], that include a pattern of saccade, fixation and blinking. Electrooculography (EOG) is an inexpensive method for mobile eye movement recordings and can be implemented using wearable sensors [69]. EOG can be used as an input modality for video gaming purposes as well [70]. Modeling of 3D eye movement tasks, while a subject performs a series of natural activities, would benefit from EOG measurements in the future.

ACKNOWLEDGMENT

The first author would like to thank late Prof. W. P. Dayawansa, Texas Tech University, for his pioneering contribution to our understanding of the *geometry of LIST*. We would like to thank Dr. Stefan Glasauer from Ludwig-Maximilians University, Munich, Germany for sharing with us, data on eye and head movement and for discussions and advice.

APPENDIX A
GEODESIC CURVES OF AN ADULT HUMAN EYE AND HEAD

Adult human eye is almost spherical but not precisely so. In this appendix, we model the human eye as an ellipsoid and sketch the corresponding geodesic trajectories. In Fig. 8, a geodesic trajectory on LIST, projected on the gaze space, is shown in two colors for two different initial conditions,[20] and two different views of the gaze space. The rotation of the eye is about the center. The moment of inertia matrix is chosen as $J = diag(m_1, m_2, m_3)$, where the ratios of the parameters m_1, m_2, m_3 is chosen to match a typical adult human eye[21] (see [72]– [74]). Note that when $m_1 = m_2 = m_3$, their geodesic equations specialize to what was described in (33). Simulations for this special case has been sketched in an earlier paper [12]. It is interesting to note from Fig. 8 that a single geodesic trajectory, projected on the gaze space, repeatedly passes through the backward gaze direction.

Likewise, the geodesic curves on $SO(3)$, using the Tait-Bryan parameters, that generalizes (30), have been obtained for a typical human head (shaped like an ellipsoid).[22] The moment of inertia matrix, in body coordinates, is given by $diag(.2718, .0529, .2698)$ in $kg\ m^2$ units. The rotation of the ellipsoid is assumed to be with respect to the bottom, South Pole, of the ellipsoid.[23] The projection of the geodesic curve on the pointing space S^2, is sketched in Fig. 9. Deviating from the circular trajectory on S^2, when $m_1 = m_2 = m_3$, sketched in [12], the pointing directions from the geodesic curve appears to tumble over all possible directions. Simulation shown in Fig. 9b shows that projection of a single geodesic curve, covers practically the whole of S^2.

Remark XV: Existence of geodesic curves on a Riemannian manifold, that are not closed curves as in Figs. 8, 9, have been discussed by Boothby [45], p. 185 and by Hilbert and Cohn-Vossen [76], pp. 222–224.

APPENDIX B
ROLE OF THE POTENTIAL AND THE DAMPING FUNCTION

In the main body of this paper (section VII), we have assumed that the potential function PE is zero. It turns out that by adding a potential function, one can change the *equilibrium point* of the Euler-Lagrange's equation (52). In this appendix, we add a *damping term* to make this equilibrium

[20]We omit writing the geodesic equation, because these equations (obtained using Mathematica) is too long to be put in this paper.

[21]An adult human eye has approximately a vertical diameter of 24 mm, a horizontal diameter of 25 mm and anterior to posterior diameter of 24.5 mm. The eye can be modeled as an ellipsoid. For moment of inertia calculations, see [71].

[22]We have used an ellipsoid with horizontal diameter $6\frac{10}{16}$ in, back to front diameter $6\frac{14}{16}$ in, and height $8\frac{6}{16}$ in.

[23]To calculate the moment of inertia matrix, we use the *parallel axis theorem* [75], to shift the point of rotation from the center of mass of the ellipsoid to the south pole.

point, asymptotically stable. The main idea presented here is from [13].

We start by separating the Kinetic and the Potential energy terms in (52) as follows

$$G\ddot{\Theta} + \dot{G}\dot{\Theta} - \frac{1}{2}\dot{\Theta}^T(\nabla_\Theta G)\dot{\Theta} = \Gamma \tag{77}$$

where

$$\Gamma = -\nabla_\Theta(PE) + \tau, \tag{78}$$

and where G, Θ and τ are already defined in section VII (see Remark XI). If we choose a damping control in the form

$$\tau = -c\,G\,\dot{\Theta}, \tag{79}$$

where $c > 0$, then the state Θ would asymptotically settle down to any one of the minima of the potential energy function PE. One can drive the state to a suitable location by selecting PE appropriately. This, in essence, is what was introduced as a potential control in [13]. We state the following as a proposition from [77].

Proposition II: For the dynamical system (77), the feedback (79) minimizes the cost function

$$J(\Theta_0, \dot{\Theta}_0) = \int_0^\infty 2c^2\,KE + \Gamma^T\,G^{-1}\,\Gamma\,dt, \tag{80}$$

where Θ_0 is the initial condition on the state. When the moment of inertia matrix is $\frac{1}{4}I_{3\times3}$, one can define an external torque vector $T = M\,G^{-1}\,\Gamma$ from (61) and the cost function (80) reduces to

$$J(\Theta_0, \dot{\Theta}_0) = \int_0^\infty 2c^2\,KE + \frac{1}{4}\|T\|^2\,dt.$$

□

Note that Γ (and hence T) has contributions from the potential energy and the generalized torque. Note also that the cost function (80) has an infinite horizon.

The potential control strategy has been applied onto the human head and the results have been sketched in Figs. 13a and 13b. The potential function we have used is taken from [13] and is given by

$$PE = A\,(1 - |q^T(\Theta)\,q_0|).$$

The point q_0 is the unit quaternion, where the potential function PE is assumed to take a minimum value. We have also used a damping term given by (79), where $c = 25$. Finally the parameter A in the potential function is chosen to be 5 in order that the dynamical system (77) settles down in approximately 1 unit of time. In Fig. 13, potential control trajectories have been plotted, in the pointing space S^2, using three different scenarios (described in the caption). All rotations are assumed to be about the south pole, simulating the neck. Based on Fig. 13, it would appear that *the shape of the head did not significantly affect the shape of the potentially controlled trajectories* (evident from the blue and black curves in the Figs. 13a and 13b), but *the shape of the Donders' surface did make a difference* (evident from the red curve in Fig. 13a).

In the final part of this appendix we comment on the structure of the damping term (79). We assume that the potential function is zero and combine (77), (78) and (79), to obtain

$$G\ddot{\Theta} + (\dot{G} + cG)\dot{\Theta} - \frac{1}{2}\dot{\Theta}^T(\nabla_\Theta G)\dot{\Theta} = 0. \tag{81}$$

The following proposition can be easily verified by direct simulation.

Proposition III: Let $\Theta_c(t)$ be solution of (81) for some initial condition $\Theta_c(0) = w_0$, $\dot{\Theta}_c(0) = w_1$, where c is a parameter in (81). For every value of $c \geq 0$, $\Theta_c(t)$ traces out a portion of the geodesic curve starting from (w_0, w_1) on the state space. □

Note that by substituting $c = 0$, we obtain as solution of (81), the geodesic curve. As is evident from Figures 8 and 9, the geodesic curves do not have a stationary point. It turns out that by increasing the value of c from 0, the curve $\Theta_c(t)$ traces out only a portion of the geodesic curve, i.e. for each c the trajectory comes to a stop. This has been demonstrated in Fig. 12. We can therefore conclude that the shape of the solution curves of (81) does not change by changing coordinates, since the geodesic does not.

Proof of Proposition III: Let $\Theta_0(t)$ be solution of (81) (assuming $c = 0$) for some initial condition $\Theta_0(0) = w_0$, $\dot{\Theta}_0(0) = w_1$. Let $f(\tau)$ be a strictly monotone function and define $Y(\tau) = \Theta_0(f(\tau))$. By direct computation, one can show that $Y(\tau)$ is a solution of the equation

$$G(Y)Y'' + \dot{G}(Y)Y' - \frac{1}{2}Y'^T(\nabla_Y G(Y))Y' - \frac{f''(\tau)}{f'(\tau)}G(Y)Y' = 0, \tag{82}$$

where $'$ denotes derivative with respect to τ. Let us now choose $f(\tau)$ in such a way that $-\frac{f''(\tau)}{f'(\tau)}$ is a constant, which we set it equal to c. It would follow that

$$f(\tau) = -\frac{1}{c}\,e^{-c\tau} + d,$$

where d is the constant of integration. The function $Y(\tau)$ satisfies (81) and we write

$$Y(\tau) = \Theta_0(-\frac{1}{c}\,e^{-c\tau} + d).$$

Assuming that the solution of (81) is unique for each choices of c, it would follow that all solutions of (81) must follow the trajectory of (81) for $c = 0$. This completes the proof. □

REFERENCES

[1] D. Robinson, "The mechanics of human saccadic eye movement," *J. Physiol.*, vol. 174, no. 2, pp. 245–264, 1964.
[2] G. C. Y. Peng, T. C. Hain, and B. W. Peterson, "Predicting vestibular, proprioceptive, and biomechanical control strategies in normal and pathological head movements," *IEEE Trans. Biomed. Eng.*, vol. 46, no. 11, pp. 1269–1280, Nov. 1999.
[3] A. Isidori, *Nonlinear Control Systems*, 3rd ed. New York, NY, USA: Springer-Verlag, 1997.
[4] I. B. Wijayasinghe, E. Aulisa, U. Büttner, B. K. Ghosh, S. Glasauer, and O. Kremmyda, "Potential and optimal control of the human head/eye complex," submitted to *IEEE Trans. Control Syst. Technol.*
[5] J. B. Listing, *Beiträge zur Physiologischen Optik*. Göttingen, Germany: Vandenhoeck und Ruprecht, 1845.

[6] F. C. Donders, "Beiträge zur lehre von den bewegungen des menschlichen auges," *Holländische Beiträge Anatomischen Physiol. Wissenschaften*, vol. 1, no. 1, pp. 104–145, 1996.

[7] H. von Helmholtz. (1866). *Handbuch der Physiologischen Optik: mit 213 in den Text eingedruckten Holzschnitten und 11 Tafeln* (Allgemeine Encyclopädie der Physik). Leipzig, Germany: Voss [Online]. Available: http://books.google.com/books?id=lh58AAAAcAAJ

[8] W. P. Medendorp, J. A. M. V. Gisbergen, M. W. I. M. Horstink, and C. C. A. M. Gielen, "Donders' law in torticollis," *J. Neurophysiol.*, vol. 82, no. 5, pp. 2833–2838, 1999.

[9] P. Radau, D. Tweed, and T. Vilis, "Three dimensional eye head and chest orientations following large gaze shifts and the underlying neural strategies," *J. Neurophysiol.*, vol. 72, no. 6, pp. 2840–2852, 1994.

[10] D. Tweed, "Three dimensional model of the human eye-head saccadic system," *J. Neurophysiol.*, vol. 77, no. 2, pp. 654–666, 1997.

[11] A. H. Clarke and T. Haslwanter, "The orientation of listing's plane in microgravity," *Vis. Res.*, vol. 47, no. 25, pp. 3132–3140, 2007.

[12] B. K. Ghosh and I. B. Wijayasinghe, "Dynamics of human head and eye rotations under Donders' constraint," *IEEE Trans. Autom. Control*, vol. 57, no. 10, pp. 2478–2489, Oct. 2012.

[13] I. B. Wijayasinghe *et al.*, "Potential and optimal control of human head movement using Tait–Bryan parametrization," *Automatica*, vol. 50, no. 2, pp. 519–529, Feb. 2014.

[14] C. Martin and L. Schovanec, "Muscle mechanics and dynamics of ocular motion," *J. Math. Syst., Estimat. Control*, vol. 8, no. 2, pp. 1–15, 1998.

[15] J. Miller and D. Robinson, "A model of the mechanics of binocular alignment," *Comput. Biomed. Res.*, vol. 17, no. 5, pp. 436–470, 1984.

[16] T. Raphan, "Modeling control of eye orientation in three dimensions. I. Role of muscle pulleys in determining saccadic trajectory," *J. Physiol.*, vol. 79, no. 5, pp. 2653–2667, 1998.

[17] C. Quaia and L. Optican, "Commutative saccadic generator is sufficient to control a 3-D ocular plant with pulleys," *J. Neurophysiol.*, vol. 79, no. 6, pp. 3197–3215, 1998.

[18] F. Zajac, "Muscle and tendon: Properties, models, scaling, and application to biomechanics and motor control," *CRC Critical Rev. Biomed. Eng.*, vol. 17, no. 4, pp. 359–411, 1989.

[19] B. W. Peterson, "Current approaches and future directions to understanding control of head movement," in *Brain Mechanisms for the Integration of Posture and Movement* (Progress in Brain Research), vol. 143, S. Mori, D. G. Stuart, and M. Weisendanger, Eds. New York, NY, USA: Elsevier, 2004, pp. 367–381.

[20] A. D. Polpitiya, W. P. Dayawansa, C. F. Martin, and B. K. Ghosh, "Geometry and control of human eye movements," *IEEE Trans. Autom. Control*, vol. 52, no. 2, pp. 170–180, Feb. 2007.

[21] U. Helmke, "Notes on human eye movement," to be published.

[22] S. L. Altmann, *Rotations, Quaternions, and Double Groups*. New York, NY, USA: Dover, 2005.

[23] J. B. Kuipers, *Quaternions and Rotation Sequences*. Princeton, NJ, USA: Princeton Univ. Press, 2002.

[24] L. D. Landau and E. M. Lifshitz, *Mechanics*, 3rd ed. Oxford, U.K.: Butterworth-Heinemann, 1996.

[25] F. Dunn and I. Parberry, *3D Math Primer for Graphics and Game Develepment*, 2nd ed. Cleveland, OH, USA: CRC Press, 2011.

[26] O. M. O'Reilly, *Intermediate Dynamics for Engineers: An Unified Treatment of Newton–Euler and Lagrangian Mechanics*. Cambridge, U.K.: Cambridge Univ. Press, 2008.

[27] S. Stancin and S. Tomazic, "Angle estimation of simultaneous orthogonal rotations from 3D gyroscope measurements," *Sensors*, vol. 11, no. 9, pp. 8536–8549, 2011.

[28] L. Euler, "Problema algebraicum ob affectiones prorsus singulares memorabile," *Commentatio 407 Indicis Enestroemiani, Novi Commentarii Acad. Sci. Petropolitan*, vol. 15, no. 5, pp. 75–106, 1770.

[29] O. Rodrigues, "Des lois geometriques qui regissent les deplacements d'un syst'eme solide dans l'espace, et de la variation des coordonnees provenant de ces deplacements consideres independamment des causes qui peuvent les produire," *J. Math.*, vol. 5, pp. 380–440, Aug. 1840.

[30] S. W. Sheppard, "Quaternion from rotation matrix," *J. Guid. Control*, vol. 1, no. 3, pp. 223–224, May/Jun. 1978.

[31] O. Kremmyda, S. Glasauer, L. Guerrasio, and U. Büttner, "Effects of unilateral midbrain lesions on gaze (eye and head) movements," *Ann. New York Acad. Sci.*, vol. 1233, no. 1, pp. 71–77, 2011.

[32] S. Glasauer, M. Hoshi, U. Kempermann, T. Eggert, and U. Büttner, "Three dimensional eye position and slow phase velocity in humans with downbeat nystagmus," *J. Neurophysiol.*, vol. 89, no. 1, pp. 338–354, 2003.

[33] A. Fick, "Neue Versuche über die Augenstellungen," in *Untersuchungen zur Naturlehre des Menschen und der Thiere*, V. Moleschott, Ed., 1860, pp. 193–233.

[34] J. Leo van Hemmen, J. D. Cowan, and E. Domany, *Models of Neural Networks IV: Early Vision and Attention*, J. L. V. Hemmen, J. D. Cowan, and E. Domany, Eds. New York, NY, USA: Springer-Verlag, 2002.

[35] J. L. Junkins and J. D. Turner, *Optimal Spacecraft Rotational Maneuvers*, 1st ed. Oxford, U.K.: Elsevier, 1986.

[36] B. Glenn and T. Vilis, "Violations of listing's law after large eye and head gaze shifts," *J. Neurophysiol.*, vol. 68, no. 1, pp. 309–318, 1992.

[37] M. Ceylan, D. Y. P. Henriques, D. B. Tweed, and J. D. Crawford, "Task-dependent costraints in motor control: Pinhole goggles make the head move like an eye," *J. Neurosci.*, vol. 20, no. 7, pp. 2719–2730, Apr. 2000.

[38] M. Theeuwen, L. E. Miller, and C. C. A. M. Gielen, "Are the orientations of the head and arm related during pointing movements?" *J. Motor Behavior*, vol. 25, no. 3, pp. 242–250, 1993.

[39] D. Tweed, B. Glenn, and T. Vilis, "Eye-head coordination during large gaze shifts," *J. Neurophysiol.*, vol. 73, no. 2, pp. 766–779, 1995.

[40] W. P. Medendorp, B. J. M. Melis, C. C. A. M. Gielen, and J. A. M. V. Gisbergen, "Off-centric rotation axes in natural head movements: Implications for vestibular reafference and kinematic redundancy," *J. Neurophysiol.*, vol. 79, no. 4, pp. 2025–2039, 1998.

[41] H. Misslisch, D. Tweed, and T. Vilis, "Neural constraints on eye motion in human eye-head saccades," *J. Neurophysiol.*, vol. 79, no. 2, pp. 859–869, 1998.

[42] D. Tweed, T. Haslwanter, and M. Fetter, "Optimizing gaze control in three dimensions," *Science*, vol. 281, no. 28, pp. 1363–1365, Aug. 1998.

[43] H. Weyl, *The Concept of a Riemann Surface*. Reading, MA, USA: Addison-Wesley, 2009.

[44] M. P. do Carmo, *Riemannian Geometry*. Cambridge, MA, USA: Birkhäuser, 1993.

[45] W. M. Boothby, *An Introduction to Differentiable Manifolds and Riemannian Geometry*. San Diego, CA, USA: Academic, 2003.

[46] R. M. Murray, Z. Li, and S. S. Sastry, *A Mathematical Introduction to Robotic Manipulation*. Boca Raton, FL, USA: CRC Press, 1994.

[47] H. Goldstein, *Classical Mechanics*. Reading, MA, USA: Addison-Wesley, 1980.

[48] J. W. Milnor and J. D. Stasheff, *Characteristic Classes*. Princeton, NJ, USA: Princeton Univ. Press, 1974.

[49] D. Mumford, *Algebraic Geometry I: Complex Projection Varieties*. New York, NY, USA: Springer-Verlag, 1976.

[50] M. I. Zelikin, *Control Theory and Optimization. I* (Encyclopaedia of Mathematical Sciences), vol. 86. New York, NY, USA: Springer-Verlag, 2000.

[51] B. K. Ghosh and C. F. Martin, "Homogeneous dynamical systems theory," *IEEE Trans. Autom. Control*, vol. 47, no. 3, pp. 462–472, Mar. 2002.

[52] C. Fox, *An Introduction to the Calculus of Variations*. New York, NY, USA: Dover, 2010.

[53] K. E. Cullen, "Sensory signals during active versus passive movement," *Current Opinion Neurobiol.*, vol. 14, no. 6, pp. 698–706, 2004.

[54] F. M. Lambert, D. Combes, J. Simmers, and H. Straka, "Gaze stabilization by efference copy signaling without sensory feedback during vertebrate locomotion," *Current Biol.*, vol. 22, no. 18, pp. 1649–1658, 2012.

[55] M. Sağlam, S. Glasauer, and N. Lehnen, "Vestibular and cerebellar contribution to gaze optimality," *Brain, J. Neurol.*, vol. 137, no. 4, pp. 1–15, 2014.

[56] B. Rogers and M. Graham, "Motion parallax as an independent cue for depth perception," *Perception*, vol. 8, no. 2, pp. 125–134, 1979.

[57] R. F. van der Willigen, B. J. Frost, and H. Wagner, "Depth generalization from stereo to motion parallax in owl," *J. Comput. Physiol. A*, vol. 187, no. 12, pp. 997–1007, 2002.

[58] K. Kral, "Behavioral-analytical studies of the role of head movements in depth perception in insects, birds and mammals," *Behavioural Process.*, vol. 64, no. 1, pp. 1–12, 2003.

[59] N. Ayache, *Artificial Vision for Mobile Robots: Stereo Vision and Multisensory Perception*. Cambridge, MA, USA: MIT Press, 1991.

[60] O. Faugeras, *The Geometry of Multiple Images: The Laws That Govern the Formation of Multiple Images of a Scene and Some of Their Applications*. Cambridge, MA, USA: MIT Press, 2001.

[61] X. Kuang, M. Gibson, B. E. Shi, and M. Rucci, "Active vision during coordinated head/eye movements in a humanoid robot," *IEEE Trans. Robot.*, vol. 28, no. 6, pp. 1423–1430, Dec. 2012.

[62] L. J. V. Rijn and A. V. V. D. Berg, "Binocular eye orientation during fixations: Listing's law extended to include eye vergence," *Vis. Res.*, vol. 33, nos. 5–6, pp. 691–708, 1993.
[63] E. Hering, *The Theory of Binocular Vision*, B. Bridgeman and L. Stark, Eds. New York, NY, USA: Plenum, 1868.
[64] I. B. Wijayasinghe and B. K. Ghosh, "Binocular eye tracking control satisfying Hering's law," in *Proc. 52nd IEEE Conf. Decision Control*, Firenze, Italy, Dec. 2013, pp. 6475–6480.
[65] M. Rajamuni, E. Aulisa, and B. K. Ghosh, "Control problems in binocular vision," in *Proc. 19th World Congr. Int. Federation Autom. Control*, Cape Town, South Africa, Aug. 2014.
[66] E. W. Justh and P. S. Krishnaprasad, "Steering laws for motion camouflage," *Proc. Roy. Soc. London Ser. B, Biol. Sci.*, vol. 462, no. 2076, pp. 3629–3643, 2006.
[67] M. V. Srinivasan and M. Davey, "Strategies for active camouflage of motion," *Proc. Roy. Soc. London. Ser. B, Biol. Sci.*, vol. 259, no. 1354, pp. 19–25, 1995.
[68] A. Bulling, J. A. Ward, H. Gellersen, and G. Tröster, "Eye movement analysis for activity recognition using electrooculography," *IEEE Trans. Pattern Anal. Mach. Intell.*, vol. 33, no. 4, pp. 741–753, Apr. 2011.
[69] A. Bulling, D. Roggen, and G. Tröster, "Wearable EOG goggles: Seamless sensing and context-awareness in everyday environments," *J. Ambient Intell. Smart Environ.*, vol. 1, no. 2, pp. 157–171, Apr. 2009.
[70] A. Bulling, D. Roggen, and G. Tröster, "Eyemote—Towards context-aware gaming using eye movements recorded from wearable electrooculography," in *Fun and Games* (Lecture Notes in Computer Science), P. Markopoulos, B. de Ruyter, W. I. Jsselsteijn, and D. Rowland, Eds. Berlin, Germamy: Springer-Verlag, 2008, pp. 33–45.
[71] H. Goldstein, C. Poole, and J. Safko, *Classical Mechanics*, 3rd ed. San Francisco, CA, USA: Addison-Wesley, 2000.
[72] *Glencoe Health*, 2nd ed., Glencoe Inc., Mission Hills, CA, USA, 1989.
[73] *Encyclopedia Britannica Macropedia: Sensory Reception*. Chicago, IL, USA: Britannica, 1997.
[74] *Magill's Medical Guide*. Winston-Salem, NC, USA: Brain Salem Press, 1998.
[75] T. R. Kane and D. A. Levinson, *Dynamics, Theory and Application*. New York, NY, USA: McGraw-Hill, 2005.
[76] D. Hilbert and S. Cohn-Vossen, *Geometry and the Imagination*. Providence, RI, USA: AMS Chelsea Publishing, 1999.
[77] B. K. Ghosh, T. Oki, S. D. Kahagalage, and I. B. Wijayasinghe, "Asymptotically stabilizing potential control for the eye movement dynamics," in *Proc. Dyn. Syst. Control Conf.*, San Antonio, TX, USA, Oct. 2014.

BIJOY K. GHOSH received the B.Tech. and M.Tech. degrees in electrical and electronics engineering from the Birla Institute of Technology and Science, Pilani, and the IIT Kanpur, Kanpur, India, and the Ph.D. degree in engineering sciences from the Decision and Control Group, Division of Applied Sciences, Harvard University, Cambridge, MA, USA, in 1977, 1979, and 1983, respectively. From 1983 to 2007, he was with the Department of Electrical and Systems Engineering, Washington University, St. Louis, MO, USA, where he was a Professor and Director of the Center for BioCybernetics and Intelligent Systems. He is currently the Dick and Martha Brooks Regents Professor of Mathematics and Statistics at Texas Tech University, Lubbock, TX, USA. He was a recipient of the Donald P. Eckmann Award from the American Automatic Control Council in 1988, the Japan Society for the Promotion of Sciences Invitation Fellowship in 1997, a Fellow of the IEEE in 2000, and a Fellow of the International Federation of Automatic Control in 2014. Until 2013, he was an IEEE Control Systems Society Representative to the IEEE-USA's Medical Technology Policy Committee and an Editorial Board Member of the IEEE TRANSACTIONS ON COMPUTATIONAL BIOLOGY AND BIOINFORMATICS. He has held visiting positions at the Tokyo Institute of Technology and Tokyo Denki University, Japan, the University of Padova, Italy, the Royal Institute of Technology and Institut Mittag-Leffler, Stockholm, Sweden, Yale University, USA, the Technical University of Munich, Germany, and IIT Kharagpur, Kharagpur, India. His research interests are in control theory, biosystems and control, and bioinformatics.

INDIKA B. WIJAYASINGHE is a Visiting Assistant Professor with the Department of Mathematics and Statistics, Sam Houston State University, Huntsville, TX, USA. He received the B.Sc. degree in electrical and electronics engineering from the University of Peradeniya, Sri Lanka, and the Ph.D. degree in applied mathematics from Texas Tech University, Lubbock, TX, USA, in 2007 and 2013, respectively. His research interests are in control theory and biomechanics.

SANATH D. KAHAGALAGE is currently pursuing Ph.D degree with the Department of Mathematics and Statistics, Texas Tech University, Lubbock, TX, USA. He received the B.Sc. degree in mechanical and manufacturing engineering from the University of Ruhuna, Sri Lanka, in 2008. His research interests are in control theory and biomechanics.